https://doi.org/10.5194/egusphere-2025-3636
Preprint. Discussion started: 8 August 2025

A Middle Atmospheric Chemistry-Climate Model MACO: Model Description and Simulation Evaluation

Zhipeng Zhu[1,2], Limin Zhou[1], Ziniu Xiao[2]

[1]Key Laboratory of Geographic Information Science, Ministry of Education, East China Normal University, Shanghai, China

[2]State Key Laboratory of Earth System Numerical Modeling and Application, Institute of Atmospheric Physics, Chinese Academy of Sciences, Beijing, China

Correspondence to: Limin Zhou (lmzhou@geo.ecnu.edu.cn)

Abstract. Developing chemistry-climate models (CCMs) is crucial for advancing our understanding of middle atmosphere and improving whole-atmosphere weather and climate forecasting. Chemical processes play a critical role in shaping the middle atmospheric thermodynamic and dynamic structures. Therefore, CCMs require explicit representation of atmospheric chemistry and must be fully coupled to physical climate components. To this end, a new middle atmosphere chemistry module based on the atmospheric general circulation model ECHAM6 has been developed, ultimately establishing a fully coupled chemistry-radiation-dynamics CCM named MACO (Middle Atmospheric Chemistry with Ozone). This paper introduces the model framework and systematically evaluates its performance through a historical simulation (1970-2014), validated vs. reanalysis and satellite datasets. MACO demonstrates robust capabilities in simulating the key dynamical and chemical processes in the middle atmosphere. The model reasonably reproduces the climatology distributions of major

https://doi.org/10.5194/egusphere-2025-3636
Preprint. Discussion started: 8 August 2025

stratospheric chemical constituents, effectively captures the annual cycle of the Antarctic ozone hole and Arctic ozone depletion, and realistically simulates the historical evolution of stratospheric ozone and HCl. However, significant biases persist in the upper stratosphere and mesosphere. Analysis identifies two primary bias sources. First, dynamical biases, including a weak polar night jet and polar vortex, lead to a pronounced warm bias near the polar stratopause. This is likely linked to the model's moderate vertical resolution, which impacts the representation of atmospheric wave dynamics. Second, biases in the chemical scheme primarily manifest as an overestimation of CH_4 and N_2O and an underestimation of H_2O and O_3 in the upper stratosphere and mesosphere. These chemical biases are partly attributed to the omission of photolysis below 177 nm, particularly the Lyman-α line. Future model development will prioritize enhancing vertical resolution and refining the photolysis scheme to address these identified shortcomings.

1. Introduction

The middle atmosphere involves complex chemistry-radiation-dynamics interactions and is a critical component of the Earth's climate system. Understanding this region is essential for predicting long-term climate trends, including the timing of stratospheric ozone recovery and the impacts of climate change on atmospheric circulation. However, numerical modeling of the middle atmosphere requires substantial computational resources due to numerous and intricate chemical reaction processes. Consequently, early middle atmosphere models, constrained by computing

https://doi.org/10.5194/egusphere-2025-3636
Preprint. Discussion started: 8 August 2025

capabilities, excluded chemical processes and functioned solely as traditional atmospheric general circulation models (Pawson et al., 2000). With advancements in high-performance computing and rapid increases in computational power over the past two to three decades, a series of middle atmosphere models — primarily incorporating stratospheric chemistry and fully coupled with atmospheric circulation models — have been developed (Shindell et al., 1998; Rozanov et al., 2001; Austin, 2002; Tian and Chipperfield, 2005; Morgenstern et al., 2009; Horowitz et al., 2020). Models of this category are commonly termed chemistry-climate models in the literature (Eyring et al., 2006).

After over three decades of development, chemistry-climate models have evolved from initial implementations with simplified stratospheric chemistry to comprehensive descriptions of stratospheric chemical processes (Eyring et al., 2006; Morgenstern et al., 2010). To evaluate the credibility of results from these models, the World Climate Research Programme (WCRP) initiated the Chemistry-Climate Model Validation (CCMVal) project in 2003. Two assessment rounds demonstrated substantial improvements among participating models, achieving better simulations of stratospheric chemistry and ozone (Eyring et al., 2005, 2006, 2010; Morgenstern et al., 2010; Gettelman et al., 2010). CCMVal was superseded by the Chemistry-Climate Model Initiative (CCMI) (Eyring et al., 2013). To date, Phase 1 of CCMI (CCMI-1) has been largely completed. CCMI emerged from the merger of CCMVal and the Atmospheric Chemistry and Climate Model Intercomparison Project (ACCMIP; Lamarque et al., 2013). Consequently, CCMI has expanded its focus from primarily

https://doi.org/10.5194/egusphere-2025-3636
Preprint. Discussion started: 8 August 2025

stratospheric chemistry to include tropospheric chemical processes, marking the advancement of chemistry-climate models toward whole-atmosphere chemistry research. Many models participating in CCMI-1 have begun refining the description of tropospheric chemistry (Eyring et al., 2013; Morgenstern et al., 2017). Simultaneously, significant enhancements were implemented in the physical and chemical parameterizations within these models, such as updates to the physical parameterization schemes, adoption of online photolysis calculation schemes, and online computation of the radiative effects due to volcanic aerosols (Morgenstern et al., 2017). Development trajectories of these CCMI-1 models indicate that updating the atmospheric general circulation model component within chemistry-climate models enhances the simulation of dynamical and physical processes. Furthermore, implementing online photolysis calculation schemes is a critical aspect requiring attention during the development of chemistry-climate models.

Photolysis is the key driver of chemical processes in the middle atmosphere, governing changes in atmospheric composition. Consequently, accurate calculation of photolysis rates (J) is critical. Two common methods for computing photolysis rates in chemistry-climate models are the online and offline approaches. The online method solves the radiative transfer equations in real time to derive photolysis rates, substantially increasing computational demands in three-dimensional atmospheric chemistry models. The offline method typically refers to the look-up table method, which provides required photolysis rates using precomputed tables and interpolation. These tables express photolysis rates as functions of pressure, solar zenith angle, ozone

https://doi.org/10.5194/egusphere-2025-3636
Preprint. Discussion started: 8 August 2025

column density, oxygen column density, temperature, etc., while also accounting for solar irradiance variability (e.g., Lary and Pyle, 1991; Rozanov et al., 1999). After being read by the numerical program, interpolation yields photolysis rates for any time and location during simulations, making the look-up table method highly efficient. Previously, most models predominantly utilized this method (Morgenstern et al., 2010), and even among recent models participating in CCMI-1, many still employ it (Morgenstern et al., 2017). However, the offline method has significant limitations: it cannot adequately capture real-time feedbacks from clouds, tropospheric aerosols, stratospheric aerosols, surface albedo, solar activity, and other factors affecting photolysis rates. Thus, corrections are often required when using look-up tables method. Sukhodolov et al. (2016) compared four look-up table methods against a reference line-by-line integration scheme, finding significant biases in the lower stratosphere and especially pronounced biases in the upper stratosphere to mesosphere, with the largest biases occurring in the mesosphere. Their study also demonstrated that photolysis rate biases from look-up table calculations further induce biases in ozone and temperature. These findings suggest replacing look-up table methods with more accurate online methods to reduce computational biases. Currently, several models have transitioned to online photolysis calculations, notably exemplified by the Fast-J series developed by the team of Prather (Wild et al., 2000; Bian and Prather, 2002; Neu et al., 2007; Prather, 2015). The latest Fast-J radiation scheme, Cloud-J, retains the advantages of previous versions for online photolysis calculations while also improving the representation of cloud vertical overlap, enabling more realistic modeling of cloud vertical structures and

https://doi.org/10.5194/egusphere-2025-3636
Preprint. Discussion started: 8 August 2025

associated radiative processes (Prather, 2015). Due to computational efficiency and accuracy, the Fast-J series is now widely implemented in chemistry-climate models and chemical transport models (Telford et al., 2013; Eastham et al., 2014; Schröter et al., 2018; Horowitz et al., 2020).

Given the significant importance of developing chemistry-climate models for scientific research and application requirements, and building upon the aforementioned review of advancements and trends of model development, this study selected the open-source atmospheric general circulation model — the sixth-generation European Centre Hamburg Model (ECHAM6) — as the foundation. Based on its existing dynamical framework and physical processes, we developed a middle atmospheric chemistry module, thereby constructing the fully coupled chemistry-radiation-dynamics chemistry-climate model MACO (Middle Atmospheric Chemistry with Ozone). The objective of this paper is to introduce the fundamental framework of MACO and evaluate its performance in simulating stratospheric chemistry and climate. The remainder of this paper is structured as follows: Section 2 provides a detailed description of the MACO model. Section 3 describes the experimental design and the datasets used for evaluation, and analyzes the model's simulation of middle atmospheric dynamics and chemistry through a comprehensive evaluation of climatology, variability, and long-term trends. Finally, Section 4 synthesizes the model performance assessment and outlines potential pathways for future model improvement.

2. Model description

The chemistry-climate model MACO consists of two components: the

https://doi.org/10.5194/egusphere-2025-3636
Preprint. Discussion started: 8 August 2025

atmospheric component model ECHAM6 and a newly developed middle atmosphere chemistry module. These components are fully coupled, allowing for two-way interaction between atmospheric chemistry, radiation and dynamics. Following specifications from CMIP6 and CCMI-2022 (Eyring et al., 2016; Plummer et al., 2021), this study established corresponding boundary conditions and external forcings modules.

2.1 Atmospheric general circulation model ECHAM6

The atmospheric component of MACO is ECHAM6.1. ECHAM6 is the sixth-generation atmospheric general circulation model developed by the Max Planck Institute for Meteorology (MPI-M) (Stevens et al., 2013). Its dynamical core retains consistency with ECHAM5, utilizing spectral truncation with spherical harmonics. To accommodate the substantial computational demands of chemistry-climate modeling under current resource constraints, MACO employs a low-resolution configuration of ECHAM6: T63 horizontal resolution (approximately 1.9°×1.9°) and 47 vertical levels (L47) extending from the surface to 0.01 hPa (approximately 80 km) using a hybrid σ-p vertical coordinate system.

ECHAM6 features several key updates compared to its predecessor, ECHAM5. The shortwave radiation scheme has been replaced with the Rapid Radiative Transfer Model for GCMs (RRTMG), which, like the longwave scheme, employs the correlated-k method (Iacono et al., 2008). The surface albedo parameterization has also been updated based on the work of Brovkin et al. (2013). Furthermore, ECHAM6 incorporates substantial improvements for representing the middle atmosphere, which

https://doi.org/10.5194/egusphere-2025-3636
Preprint. Discussion started: 8 August 2025

are detailed in Stevens et al. (2013).

The model's transport scheme handles several processes. The advection of chemical species is managed by the flux-form semi-Lagrangian scheme of Lin and Rood (1996). Turbulent mixing is treated using the eddy diffusion and viscosity approach from Brinkop and Roeckner (1995). Moist convection is parameterized according to Tiedtke (1989), with subsequent extensions by Nordeng (1994) and Moebis and Stevens (2012). Gravity wave drag (GWD) is split into two components: the orographic GWD uses the subgrid-scale parameterization of Lott (1999), with wave propagation and dissipation following Palmer et al. (1986) and Miller et al. (1989), while the parameterization of non-orographic GWD is based on the Doppler spread theory described by Hines (1997a, 1997b). The land-surface component of ECHAM6 is the Jena Scheme for Biosphere-Atmosphere Coupling in Hamburg (JSBACH), which provides the lower boundary conditions over land and simulates processes such as soil and litter decomposition, and land-use change (Reick et al., 2013).

Overall, ECHAM6 shows improved performance over ECHAM5 in several key areas, most notably in the mid-latitudes. ECHAM6 also demonstrates skill in simulating tropical variability, including intraseasonal oscillations and the stratospheric quasi-biennial oscillation (QBO).

2.2 Middle atmosphere chemistry module

The middle atmosphere chemistry module implements numerical formulations for chemical processes in the middle atmosphere and achieves two-way coupling with ECHAM6. This module formulates a chemical mechanism appropriate for the middle

https://doi.org/10.5194/egusphere-2025-3636
Preprint. Discussion started: 8 August 2025

atmosphere. This mechanism comprises five chemical families (O_x, NO_x, HO_x, ClO_x, BrO_x), CH_4 and its derivatives, totaling 48 chemical species (see Table 1), involving 46 photolysis reactions, 123 gas-phase reactions, and 11 stratospheric heterogeneous reactions (see Tables 2-4). All reaction rate coefficients, absorption cross-sections, and parameters for heterogeneous reaction processes follow the recommendations provided in the 2019 evaluation report (Burkholder et al., 2019) by the NASA Jet Propulsion Laboratory (JPL).

Table 1. Chemical components in the MACO model

No.	Species	Note	No.	Species	Note
1	Br		25	ClO	
2	Br_2		26	$ClONO_2$	
3	BrCl		27	H	
4	BrO		28	H_2	
5	$BrONO_2$		29	H_2O	
6	$CBrF_3$	H-1301	30	H_2O_2	
7	CCl_2F_2	CFC-12	31	HBr	
8	CCl_2FCClF_2	CFC-113	32	HCl	
9	CCl_3F	CFC-11	33	HNO_3	
10	CCl_4		34	HO_2	
11	$CClBrF_2$	H-1211	35	HO_2NO_2	
12	CH_2O		36	HOBr	
13	CH_3Br		37	HOCl	
14	CH_3CCl_3		38	N	
15	CH_3Cl		39	N_2O	
16	CH_3O_2		40	N_2O_5	
17	CH_3OOH		41	NO	
18	CH_4		42	NO_2	
19	$CHClF_2$	HCFC-22	43	NO_3	
20	CO		44	O	
21	Cl		45	$O(^1D)$	
22	Cl_2		46	O_3	
23	Cl_2O_2		47	OClO	
24	$ClNO_2$		48	OH	

https://doi.org/10.5194/egusphere-2025-3636
Preprint. Discussion started: 8 August 2025

190

Table 2. Photolysis reactions in the MACO model

No.	Reactions	No.	Reactions
1	$O_2 + h\nu \rightarrow 2O$	24	$Cl_2O_2 + h\nu \rightarrow 2Cl$
2	$O_3 + h\nu \rightarrow O(^1D) + O_2$	25	$HOCl + h\nu \rightarrow OH + Cl$
3	$O_3 + h\nu \rightarrow O + O_2$	26	$ClONO_2 + h\nu \rightarrow Cl + NO_3$
4	$N_2O + h\nu \rightarrow O(^1D) + N_2$	27	$ClONO_2 + h\nu \rightarrow ClO + NO_2$
5	$NO + h\nu \rightarrow N + O$	28	$BrCl + h\nu \rightarrow Br + Cl$
6	$NO_2 + h\nu \rightarrow NO + O$	29	$BrO + h\nu \rightarrow Br + O$
7	$N_2O_5 + h\nu \rightarrow NO_2 + NO_3$	30	$HOBr + h\nu \rightarrow Br + OH$
8	$N_2O_5 + h\nu \rightarrow NO + O + NO_3$	31	$BrONO_2 + h\nu \rightarrow Br + NO_3$
9	$HNO_3 + h\nu \rightarrow NO_2 + OH$	32	$BrONO_2 + h\nu \rightarrow BrO + NO_2$
10	$NO_3 + h\nu \rightarrow NO_2 + O$	33	$CH_3Cl + h\nu \rightarrow Cl + CH_3O_2$
11	$NO_3 + h\nu \rightarrow NO + O_2$	34	$CCl_4 + hv \rightarrow 4Cl$
12	$HO_2NO_2 + h\nu \rightarrow OH + NO_3$	35	$CH_3CCl_3 + h\nu \rightarrow 3Cl$
13	$HO_2NO_2 + h\nu \rightarrow NO_2 + HO_2$	36	$CCl_3F + h\nu \rightarrow 3Cl$
14	$CH_3OOH + h\nu \rightarrow CH_2O + HO_2 + OH$	37	$CCl_2F_2 + h\nu \rightarrow 2Cl$
15	$CH_2O + h\nu \rightarrow CO + HO_2 + H$	38	$CCl_2FCClF_2 + h\nu \rightarrow 3Cl$
16	$CH_2O + h\nu \rightarrow CO + H_2$	39	$CHClF_2 + h\nu \rightarrow Cl$
17	$H_2O + h\nu \rightarrow OH + H$	40	$CH_3Br + h\nu \rightarrow Br + CH_3O_2$
18	$H_2O + h\nu \rightarrow H_2 + O(^1D)$	41	$CBrF_3 + h\nu \rightarrow Br$
19	$H_2O + h\nu \rightarrow 2H + O$	42	$CClBrF_2 + h\nu \rightarrow Br + Cl$
20	$H_2O_2 + h\nu \rightarrow 2OH$	43	$HCl + h\nu \rightarrow H + Cl$
21	$Cl_2 + h\nu \rightarrow 2Cl$	44	$HBr + h\nu \rightarrow H + Br$
22	$ClO + h\nu \rightarrow Cl + O$	45	$ClNO_2 + h\nu \rightarrow Cl + NO_2$
23	$OClO + h\nu \rightarrow O + ClO$	46	$Br_2 + h\nu \rightarrow 2Br$

195

https://doi.org/10.5194/egusphere-2025-3636
Preprint. Discussion started: 8 August 2025

Table 3. Gas-phase reactions in the MACO model

No.	Reactions	No.	Reactions
1	$O + O_2 + M \rightarrow O_3 + M$	63	$Cl + H_2 \rightarrow HCl + H$
2	$O + O_3 \rightarrow O_2 + O_2$	64	$Cl + H_2O_2 \rightarrow HCl + HO_2$
3	$O + O + M \rightarrow O_2 + M$	65	$Cl + HO_2 \rightarrow HCl + O_2$
4	$O(^1D) + N_2 \rightarrow O + N_2$	66	$Cl + HO_2 \rightarrow OH + ClO$
5	$O(^1D) + O_2 \rightarrow O + O_2$	67	$Cl + CH_2O \rightarrow HCl + HO_2 + CO$
6	$O(^1D) + H_2O \rightarrow OH + OH$	68	$Cl + CH_4 \rightarrow CH_3O_2 + HCl$
7	$O(^1D) + N_2O \rightarrow N_2 + O_2$	69	$ClO + O \rightarrow Cl + O_2$
8	$O(^1D) + N_2O \rightarrow NO + NO$	70	$ClO + OH \rightarrow Cl + HO_2$
9	$O(^1D) + O_3 \rightarrow 0.5O_2 + 0.5O_2 + 0.5O_2 + O$	71	$ClO + OH \rightarrow HCl + O_2$
10	$O(^1D) + CCl_3F \rightarrow 3Cl$	72	$ClO + HO_2 \rightarrow O_2 + HOCl$
11	$O(^1D) + CCl_2F_2 \rightarrow 2Cl$	73	$ClO + CH_3O_2 \rightarrow Cl + HO_2 + CH_2O$
12	$O(^1D) + CCl_2FCClF_2 \rightarrow 3Cl$	74	$ClO + NO \rightarrow NO_2 + Cl$
13	$O(^1D) + CHClF_2 \rightarrow Cl$	75	$ClO + ClO \rightarrow 2Cl + O_2$
14	$O(^1D) + CCl_4 \rightarrow 4Cl$	76	$ClO + ClO \rightarrow Cl_2 + O_2$
15	$O(^1D) + CH_3Br \rightarrow Br$	77	$ClO + ClO \rightarrow Cl + OClO$
16	$O(^1D) + CClBrF_2 \rightarrow Cl + Br$	78	$HCl + OH \rightarrow H_2O + Cl$
17	$O(^1D) + CBrF_3 \rightarrow Br$	79	$HCl + O \rightarrow Cl + OH$
18	$O(^1D) + CH_4 \rightarrow CH_3O_2 + OH$	80	$HOCl + O \rightarrow ClO + OH$
19	$O(^1D) + CH_4 \rightarrow CH_2O + H + HO_2$	81	$HOCl + Cl \rightarrow Cl_2 + OH$
20	$O(^1D) + CH_4 \rightarrow CH_2O + H_2$	82	$HOCl + OH \rightarrow H_2O + ClO$
21	$O(^1D) + H_2 \rightarrow OH + H$	83	$ClONO_2 + O \rightarrow ClO + NO_3$
22	$O(^1D) + HCl \rightarrow Cl + OH$	84	$ClONO_2 + OH \rightarrow HOCl + NO_3$
23	$O(^1D) + HBr \rightarrow Br + OH$	85	$ClONO_2 + Cl \rightarrow Cl_2 + NO_3$
24	$N + O_2 \rightarrow NO + O$	86	$O + OClO \rightarrow ClO + O_2$
25	$N + NO \rightarrow N_2 + O$	87	$OH + OClO \rightarrow HOCl + O_2$
26	$N + NO_2 \rightarrow N_2O + O$	88	$NO + OClO \rightarrow NO_2 + ClO$
27	$H + NO_2 \rightarrow OH + NO$	89	$Cl + OClO \rightarrow ClO + ClO$
28	$NO + HO_2 \rightarrow NO_2 + OH$	90	$ClO + ClO + M \rightarrow Cl_2O_2 + M$
29	$NO + O_3 \rightarrow NO_2 + O_2$	91	$Cl_2O_2 + M \rightarrow ClO + ClO + M$
30	$NO_2 + O_3 \rightarrow NO_3 + O_2$	92	$ClO + NO_2 + M \rightarrow ClONO_2 + M$
31	$NO_3 + NO \rightarrow 2NO_2$	93	$Br + O_3 \rightarrow BrO + O_2$
32	$NO_3 + O \rightarrow NO_2 + O_2$	94	$Br + HO_2 \rightarrow HBr + O_2$
33	$NO_3 + OH \rightarrow HO_2 + NO_2$	95	$Br + CH_2O \rightarrow HBr + HO_2 + CO$
34	$NO_3 + HO_2 \rightarrow OH + NO_2 + O_2$	96	$BrO + O \rightarrow Br + O_2$
35	$HO_2NO_2 + OH \rightarrow H_2O + NO_2 + O_2$	97	$BrO + OH \rightarrow Br + HO_2$
36	$NO + O + M \rightarrow NO_2 + M$	98	$BrO + HO_2 \rightarrow HOBr + O_2$
37	$NO_2 + O + M \rightarrow NO_3 + M$	99	$BrO + NO \rightarrow Br + NO_2$
38	$NO_2 + O + M \rightarrow NO + O_2$	100	$BrO + ClO \rightarrow Br + OClO$
39	$NO_2 + NO_3 + M \rightarrow N_2O_5 + M$	101	$BrO + ClO \rightarrow Br + Cl + O_2$

https://doi.org/10.5194/egusphere-2025-3636
Preprint. Discussion started: 8 August 2025

Table 3. Continued

No.	Reactions	No.	Reactions
40	$N_2O_5 + M \rightarrow NO_2 + NO_3 + M$	102	$BrO + ClO \rightarrow BrCl + O_2$
41	$NO_2 + HO_2 + M \rightarrow HO_2NO_2 + M$	103	$BrO + BrO \rightarrow 2Br + O_2$
42	$HO_2NO_2 + M \rightarrow HO_2 + NO_2 + M$	104	$HBr + OH \rightarrow Br + H_2O$
43	$NO_2 + OH + M \rightarrow HNO_3 + M$	105	$HBr + O \rightarrow Br + OH$
44	$HNO_3 + OH + M \rightarrow NO_3 + H_2O$	106	$HOBr + O \rightarrow BrO + OH$
45	$H + O_3 \rightarrow OH + O_2$	107	$BrONO_2 + O \rightarrow BrO + NO_3$
46	$H + HO_2 \rightarrow OH + OH$	108	$BrO + NO_2 + M \rightarrow BrONO_2 + M$
47	$H + HO_2 \rightarrow H_2 + O_2$	109	$CH_3Cl + Cl \rightarrow HO_2 + CO + 2HCl$
48	$H + HO_2 \rightarrow H_2O + O$	110	$CH_3Cl + OH \rightarrow Cl + H_2O + HO_2$
49	$OH + O \rightarrow H + O_2$	111	$CH_3CCl_3 + OH \rightarrow H_2O + 3Cl$
50	$OH + O_3 \rightarrow HO_2 + O_2$	112	$CHClF_2 + OH \rightarrow Cl + H_2O$
51	$OH + HO_2 \rightarrow H_2O + O_2$	113	$CH_3Br + OH \rightarrow Br + H_2O + HO_2$
52	$OH + OH \rightarrow H_2O + O$	114	$CH_3Br + Cl \rightarrow HCl + HO_2 + Br$
53	$OH + H_2 \rightarrow H_2O + H$	115	$CH_4 + OH \rightarrow CH_3O_2 + H_2O$
54	$OH + H_2O_2 \rightarrow H_2O + HO_2$	116	$CH_3O_2 + NO \rightarrow CH_2O + NO_2 + HO_2$
55	$H_2 + O \rightarrow OH + H$	117	$CH_3O_2 + HO_2 \rightarrow CH_3OOH + O_2$
56	$HO_2 + O \rightarrow OH + O_2$	118	$CH_2O + NO_3 \rightarrow CO + HO_2 + HNO_3$
57	$HO_2 + O_3 \rightarrow OH + 2O_2$	119	$CH_2O + OH \rightarrow CO + H_2O + HO_2$
58	$HO_2 + HO_2 \rightarrow H_2O_2 + O_2$	120	$CH_2O + O \rightarrow HO_2 + OH + CO$
59	$H_2O_2 + O \rightarrow OH + HO_2$	121	$CH_3OOH + OH \rightarrow 0.7CH_3O_2 + 0.3OH + 0.3CH_2O + H_2O$
60	$H + O_2 + M \rightarrow HO_2 + M$	122	$CO + OH + M \rightarrow CO_2 + HO_2 + M$
61	$OH + OH + M \rightarrow H_2O_2 + M$	123	$CO + OH + M \rightarrow CO_2 + H$
62	$Cl + O_3 \rightarrow ClO + O_2$		

200

Table 4. Stratospheric heterogeneous reactions in the MACO model

No.	Reactions	No.	Reactions
1	$N_2O_5 + H_2O \rightarrow 2HNO_3$	7	$BrONO_2 + HCl \rightarrow BrCl + HNO_3$
2	$N_2O_5 + HCl \rightarrow ClNO_2 + HNO_3$	8	$HOCl + HCl \rightarrow Cl_2 + H_2O$
3	$ClONO_2 + H_2O \rightarrow HOCl + HNO_3$	9	$HOCl + HBr \rightarrow BrCl + H_2O$
4	$ClONO_2 + HCl \rightarrow Cl_2 + HNO_3$	10	$HOBr + HCl \rightarrow BrCl + H_2O$
5	$ClONO_2 + HBr \rightarrow BrCl + HNO_3$	11	$HOBr + HBr \rightarrow Br_2 + H_2O$
6	$BrONO_2 + H_2O \rightarrow HOBr + HNO_3$		

https://doi.org/10.5194/egusphere-2025-3636
Preprint. Discussion started: 8 August 2025

Numerical solution of the chemical system — a coupled set of ordinary differential equations (ODEs) — provides the tendency terms for composition changes due to photochemistry. This stiff ODE system necessitates complex coding for both the ODEs and their associated linear algebraic solvers. To address this challenge, the module utilizes the open-source Kinetic PreProcessor (KPP) software developed by Sandu and Sander (2006), to automate module code generation. The generated code is subsequently adapted to meet specific model requirements. KPP is widely utilized in implementing chemical processes for multiple international atmospheric chemistry models. It enables automated code generation, which significantly reduces manual programming efforts and associated errors, enabling streamlined updates to chemical mechanisms and replacements/upgrades of numerical solvers for chemical operators. The module employs the Rosenbrock method, a non-iterative implicit solver particularly well-suited for stiff systems, as the numerical solver for chemical operators.

Photolysis rates are calculated online using the radiative transfer model Cloud-J version 7.3 developed by Prather (2015). Cloud-J uses an eight-stream Fourier multiple-scattering method, dividing solar radiation between 177 and 778 nm into 18 spectral bins: 11 bins for the stratospheric region (177-290 nm) and 7 bins for the tropospheric region (290-778 nm). Cloud-J primarily accounts for O_2 and O_3 absorption, Rayleigh scattering, and Mie scattering by clouds and aerosols. Cloud-J is suitable for photolysis calculations at altitudes below approximately 60 km. Stratospheric photolysis processes primarily occur at radiation wavelengths above 177 nm. However, radiation below 177 nm (primarily the Lyman-α line) becomes important for some species like CH_4, H_2O,

https://doi.org/10.5194/egusphere-2025-3636
Preprint. Discussion started: 8 August 2025

and O_2 in the upper stratosphere and mesosphere. Existing approaches for handling wavelengths below 177 nm have been described by Telford et al. (2013), who implemented the online Fast-JX scheme in the UK Chemistry and Aerosols model (UKCA), while utilizing the offline scheme from Lary and Pyle (1991) to compute photolysis rates above 0.2 hPa as a method to specifically address this spectral region. However, research by Sukhodolov et al. (2016) indicates inadequate performance of this offline scheme for H_2O and O_2 photolysis calculations above 60 km. Selection of a more reliable offline scheme is therefore essential. As both scheme selection and its implementation in the model require substantial effort, this initial model version does not include photolysis processes below 177 nm, and this component will be refined in future versions. Model evaluation in Section 3 identifies the absence of this spectral band as a partial cause of simulation biases near the stratopause. However, quantitative assessment of error contributions requires dedicated model development and sensitivity experiment design, which warrants further research.

Stratospheric heterogeneous reactions primarily occur at the interfaces of solid and liquid particles, such as polar stratospheric clouds (PSCs) and sulfate aerosols. Simulation of heterogeneous reactions in polar stratospheric regions requires specification of PSC physical parameters. PSCs are classified into three types: PSC-1a consists of nitric acid trihydrate (NAT), PSC-1b consists of supercooled ternary solution (STS) droplets, and PSC-2 consists of water ice. The presence of PSCs is a necessary condition for polar ozone depletion during spring. This module simulates PSCs formation and gravitational sedimentation using the parameterization documented by

https://doi.org/10.5194/egusphere-2025-3636
Preprint. Discussion started: 8 August 2025

Kirner et al. (2011), which defines the potential PSC formation region as 45°N-90°N in the Northern Hemisphere, 55°S-90°S in the Southern Hemisphere, and between 180 and 5 hPa vertically; PSCs cannot form outside these regions. The STS is parameterized follows the scheme by Carslaw et al. (1995), describing the uptake of HNO_3 and some halogen species by sulfuric acid aerosols to form STS. The parameterization of the uptake coefficients for liquid-phase reactions uses the method from Carslaw et al. (1997). For NAT, the module employs the thermodynamic parameterization method proposed by Hanson and Mauersberger (1988), whereby NAT formation occurs via heterogeneous nucleation on preexisting solid PSCs when HNO_3 partial pressure exceeds its saturation vapor pressure. The simulation sequence prioritizes NAT formation before STS uptake of HNO_3. Water ice formation follows the thermodynamic parameterization established by Marti and Mauersberger (1993), with concentration derived from the difference between H_2O partial pressure and its saturation vapor pressure. Denitrification and dehydration result from gravitational settling of NAT and water ice particles, simulated using the trapezoidal scheme from Buchholz (2005). Notably, water ice and NAT particles do not undergo explicit transport. Instead, they re-evaporate into gaseous H_2O and HNO_3 after each chemical time step and subsequently transported in gaseous form. At the next time step, these particles are regenerated anew based on the updated saturation conditions through the aforementioned thermodynamic equilibrium assumptions.

Dry deposition simulation adopts a one-way sedimentation scheme occurring exclusively at the model lowermost layer, assuming irreversible deposition where the

https://doi.org/10.5194/egusphere-2025-3636
Preprint. Discussion started: 8 August 2025

surface acts as the ultimate sink. The current model version utilizes simplified dry deposition calculation by predefining constant deposition velocity values. The module includes dry deposition processes for CO, NO, NO_2, O_3, HNO_3, H_2O_2, and H_2. Dry deposition velocities over land and ocean originate from data compiled by Hauglustaine et al. (1994) and Hauglustaine and Ehhalt (2002) (see Table 5).

Wet deposition processes are categorized by physical mechanism into in-cloud scavenging (rainout) and below-cloud scavenging (washout). The module simulates wet deposition using the scheme introduced by Brasseur et al. (1998), currently applied to 10 chemical species: HNO_3, H_2O_2, HCl, HOCl, $ClONO_2$, HBr, HOBr, $BrONO_2$, CH_2O, and CH_3OOH.

Table 5. Dry deposition velocities of chemical species (units: cm/s)

Species	Land	Ocean
CO	0.03	0
NO	0.016	0.003
NO_2	0.1	0.02
O_3	0.4	0.07
HNO_3	4.0	1.0
H_2O_2	0.5	1.0

2.3 Model Configuration and Boundary Conditions

MACO establishes three-dimensional chemical-radiative-dynamical coupling between the middle atmosphere chemistry module and ECHAM6, as described previously. The chemical transport processes for all species in the middle atmosphere

https://doi.org/10.5194/egusphere-2025-3636
Preprint. Discussion started: 8 August 2025

chemistry module are simulated via the ECHAM6 dynamical transport module, which handles advection, turbulent mixing, and vertical convection. The advective transport employs the flux-form semi-Lagrangian scheme, namely the Lin-Rood scheme (Lin and Rood, 1996). Radiative transfer calculations utilize H_2O, O_3, CH_4, N_2O, CFC-11, and CFC-12 concentrations provided in real time by the middle atmosphere chemistry module. Radiation transfer calculations and chemistry system solvers are executed every two hours.

Following the implementation of Cloud-J for online photolysis rate calculations, Cloud-J can acquire cloud-related parameters such as cloud fraction on each vertical layer simulated by the model in real-time. It establishes a cloud overlap model to calculate the influence of cloud layers on photolysis rates. Cloud-J offers eight schemes for cloud model settings in radiation transfer calculations. To realistically simulate the cloud overlap effect on photolysis rates, the AvQCA scheme is selected as the default option, following recommendations by Prather (2015). The AvQCA scheme employs the maximum-correlated overlap model for cloud vertical overlap and computes average photolysis rates across generated independent atmospheric columns via the Average in each Quadrature Column Atmospheres (AvQCA) method. This scheme relies on cloud physical parameters defined on model layers. Detailed descriptions of Cloud-J cloud model schemes are available in Prather (2015).

Emission inventory data are ingested offline to the model for calculating pollutant concentrations from anthropogenic and natural sources. Aircraft emission fluxes are interpolated to corresponding model layers, while all other emissions are specified as

https://doi.org/10.5194/egusphere-2025-3636
Preprint. Discussion started: 8 August 2025

fluxes at the model lowermost layer. The model focuses on anthropogenic emissions and biomass burning. Global anthropogenic emissions come from the Community Emissions Data System (CEDS) dataset (Hoesly et al., 2018), while global biomass burning emissions originate from van Marle et al. (2017). Both inventories are recommended for CMIP6 and CCMI-2022 experiments. The chemical species currently considered from anthropogenic and biomass burning sources are CO and nitrogen oxides ($NO_x = NO + NO_2$). Non-methane volatile organic compounds and other species critical for tropospheric chemistry are excluded, as the core chemical mechanism targets the middle atmosphere. Emissions of NO_x from natural biogenic sources and lightning are also omitted currently. These emissions are more crucial for tropospheric chemistry but exhibit high sensitivity to meteorological and climatic variations; thus, it is preferable to employ interactive parameterization methods that allow the model to diagnose these emissions online (Plummer et al., 2021). Such interactive parameterization scheme requires further model development and will be implemented in future model versions.

Representing the quasi-biennial oscillation (QBO), a key interannual variability signal in the tropical stratosphere, is essential for understanding ozone and other trace species variability in tropical and extratropical middle atmosphere. Since the model uses a low-resolution version of ECHAM6, its vertical resolution is insufficient to accurately simulate the realistic QBO. The model adopts the QBO nudging scheme proposed by Giorgetta (1996) based on Newtonian relaxation principles to nudge stratospheric zonal winds in the tropics toward observed equatorial wind profiles from

https://doi.org/10.5194/egusphere-2025-3636
Preprint. Discussion started: 8 August 2025

Plummer et al. (2021), thereby improving QBO simulation. The nudging scheme is applied with minor adjustments following Stenke et al. (2013), with nudging occurring in the latitude range of 20°S-20°N and the vertical range of 3-90 hPa.

The global monthly mean sea surface temperature (SST) and sea ice coverage (SIC) dataset used by the model is the HadISST1 dataset provided by the UK Met Office Hadley Centre (Rayner et al., 2003). Greenhouse gas and ozone depleting substances (ODSs) forcings are sourced from Meinshausen et al. (2017). Greenhouse gases mainly include CO_2, CH_4, and N_2O. ODSs includes ten species: CFC-11, CFC-12, CFC-113, CH_3CCl_3, CCl_4, CH_3Cl, CH_3Br, HCFC-22, Halon-1211, and Halon-1301. All greenhouse gases and ODSs, except CO_2, are specified as lower boundary conditions, while CO_2 uses a uniform value throughout the three-dimensional domain. Solar radiation forcing uses solar spectral irradiance data from Matthes et al. (2017), from which the top-of-atmosphere actinic flux data for photolysis are computed. Stratospheric aerosol forcing uses data from Kovilakam et al. (2020). Calculating volcanic aerosol radiative effects requires extinction coefficients, asymmetry factors, and single-scattering albedos provided by the dataset. Calculation of stratospheric heterogeneous reactions utilizes the volcanic aerosol volume density and sulfuric acid number concentration provided in the dataset. All the forcing data mentioned above are recommended for CMIP6. Tropospheric aerosol forcing follows the ECHAM6 scheme, utilizing the tropospheric aerosol optical parameter data from Kinne et al. (2013) to calculate radiative forcing.

3 Evaluation of MACO

https://doi.org/10.5194/egusphere-2025-3636
Preprint. Discussion started: 8 August 2025

3.1 Numerical experiments design and dataset for model evaluation

To evaluate the model simulation performance, historical simulation experiments were conducted. The boundary condition data required for model operation vary with time, and specific details regarding these data and model configuration have been described in Section 2.3. The simulation period spans from 1970 to 2014. The first 10 years (1970-1979) are treated as a model spin-up period, and the analysis focuses on the years 1980-2014.

The model simulation is evaluated against a comprehensive suite of observational and reanalysis datasets:

MERRA-2 (Modern-Era Retrospective Analysis for Research and Applications, Version 2) reanalysis data provided by NASA (Gelaro et al., 2017). It covers the period from 1980 to present, with a horizontal resolution of 0.5° × 0.625° and 72 vertical layers extending from the surface to 0.01 hPa. Temperature and zonal wind data from MERRA-2 are used in this analysis.

GOZCARDS (Global Ozone Chemistry and Related trace gas Data records for the Stratosphere) satellite composite data provided by NASA (Froidevaux et al., 2015). This dataset provides high-quality, long-term merged satellite records of zonal mean O_3, HCl, H_2O, HNO_3, and N_2O, with temporal coverage spanning 1984-2012, 1991-2012, 1991-2012, 2004-2012, and 2004-2012, respectively.

ACE-FTS v3.5 (Atmospheric Chemistry Experiment Fourier Transform Spectrometer, Version 3.5) data from the Canadian SCISAT satellite (Bernath et al., 2005). This analysis uses the zonal mean CH_4 data (zonal mean), covering the period

https://doi.org/10.5194/egusphere-2025-3636
Preprint. Discussion started: 8 August 2025

2004–2012.

MSR-2 (Multi-Sensor Reanalysis, Version 2) total ozone column data from van der A et al. (2015). This dataset assimilates total ozone column retrievals from 15 satellite instruments, with a horizontal resolution of 0.5° × 0.5° and temporal coverage from 1960 to 2022.

3.2 Evaluation of atmospheric dynamics

Figure 1 shows the latitude-height distributions of climatological (1980-2014) zonal mean temperatures simulated by the model for four seasons, compared with observations. Overall, the model captures the zonal-mean temperature distribution accurately, although biases occur in the middle atmosphere relative to observations. Specifically, simulated tropospheric temperatures agree well with observations, with biases below 2.5 K, except for a -2.5 to -5 K cold bias near the extratropical tropopause compared to observations. Simulated temperatures in the lower stratosphere also closely match observations, with biases generally within 2.5 K. However, larger biases appear in the simulation of the mid-upper stratosphere and mesosphere. Temperatures simulated above 0.1 hPa are higher than observations by more than 2.5-5 K throughout the year. The most pronounced differences occur between the mid-upper stratosphere and 0.1 hPa, with maximum biases near the stratopause. Additionally, between the mid-upper stratosphere and 0.1 hPa during spring (March-May) and summer (June-August), temperatures over Antarctic are 2.5-10 K higher than observations. Similarly, during autumn (September-November) and winter (December-February), temperatures over the Arctic exhibit such warm biases. The warm biases reach maxima over Antarctic in

https://doi.org/10.5194/egusphere-2025-3636
Preprint. Discussion started: 8 August 2025

summer and the Arctic in winter, respectively. Outside these regions, temperatures are generally lower than observed, with the most significant biases (exceeding 10 K) occurring over the Arctic in summer and the Antarctic in winter. The warm bias patterns over Antarctica in spring-summer and the Arctic in autumn-winter arise from a weaker simulated vortex, which enhances meridional transport and mixing. This bias is a persistent issue in ECHAM and other GCMs (Stevens et al., 2013; Gettelman et al., 2019), which can be significantly improved by using higher vertical resolution version of ECHAM at the expense of greater computational demands (Mauritsen et al., 2019). The cause of the cold bias elsewhere near the stratopause will be discussed further in the subsequent analysis of chemical process.

Figure 2 presents the latitude-height distributions of simulated zonal winds. Overall, the model reproduces the spatial pattern of observed zonal winds well. The model reasonably captures the position and intensity of tropospheric jets, with absolute biases of approximately 2-5 m/s. Differences between the model and observations increase with altitude. The simulated intensity of the summer hemisphere stratospheric easterly jet matches observations closely (Fig. 2d and j), but its shape shows minor differences. In the mesosphere, simulated easterlies are 10-20 m/s weaker than observations (Fig. 2f and l). In the stratosphere, the intensity of the simulated Southern Hemisphere polar night jet and polar vortex agrees well with observations (Fig. 2d), but their positions are shifted. The core of the Antarctic polar night jet in the simulation is near 60°S between 10-1 hPa, whereas observations place the jet core near 40°S between 3-0.1 hPa (Fig. 2e). The simulated Northern Hemisphere polar night jet closely matches

https://doi.org/10.5194/egusphere-2025-3636
Preprint. Discussion started: 8 August 2025

observations in the mid-lower stratosphere (Fig. 2j), with biases below 2.5 m/s (Fig. 2l). In the mesosphere, the westerly jets in both hemispheres are weaker than observed, with biases exceeding 10 m/s, particularly in the Southern Hemisphere (Fig. 2f and l). These weaker polar night jets and vortices correspond well to the warmer temperatures seen above the upper stratosphere in Figure 1.

As mentioned earlier, the low vertical resolution of the model prevents a satisfactory simulation of the QBO without nudging. To evaluate the nudging effect, Figure 3 analyzes the monthly evolution of tropical stratospheric zonal winds during 1995-2014. The model successfully reproduces the main characteristics of the QBO. With nudging, the model successfully simulates the periodic variation of QBO and its downward propagation into the lower stratosphere over time (Fig. 3a). However, biases relative to observations remain (Fig. 3b): in the mid-lower stratosphere, the simulated amplitude of the QBO easterly phase is weaker, while the westerly phase amplitude is stronger.

https://doi.org/10.5194/egusphere-2025-3636
Preprint. Discussion started: 8 August 2025

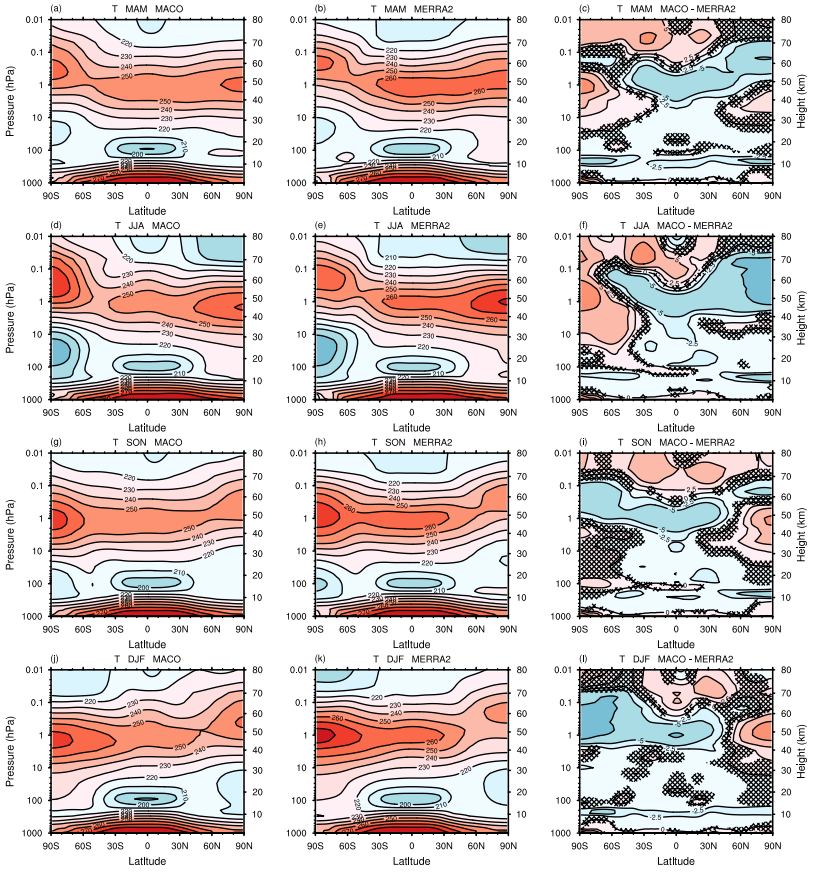

Figure 1. Latitude-altitude distributions of temperature simulated by the MACO (first column) from 1980 to 2014, temperature from the MERRA2 reanalysis data (second column), and the temperature differences between the model and MERRA2 (third column) (units: K). Panels (a-c), (d-f), (g-i), and (j-l) show results for spring, summer, autumn, and winter, respectively. In the third column, contour intervals are set at -20, -10, -5, -2.5, 0, 2.5, 5, 10, and 20. The slanted grid areas denote regions where the temperature differences are not statistically significant at the 95% confidence level based on a t-test.

https://doi.org/10.5194/egusphere-2025-3636
Preprint. Discussion started: 8 August 2025

445

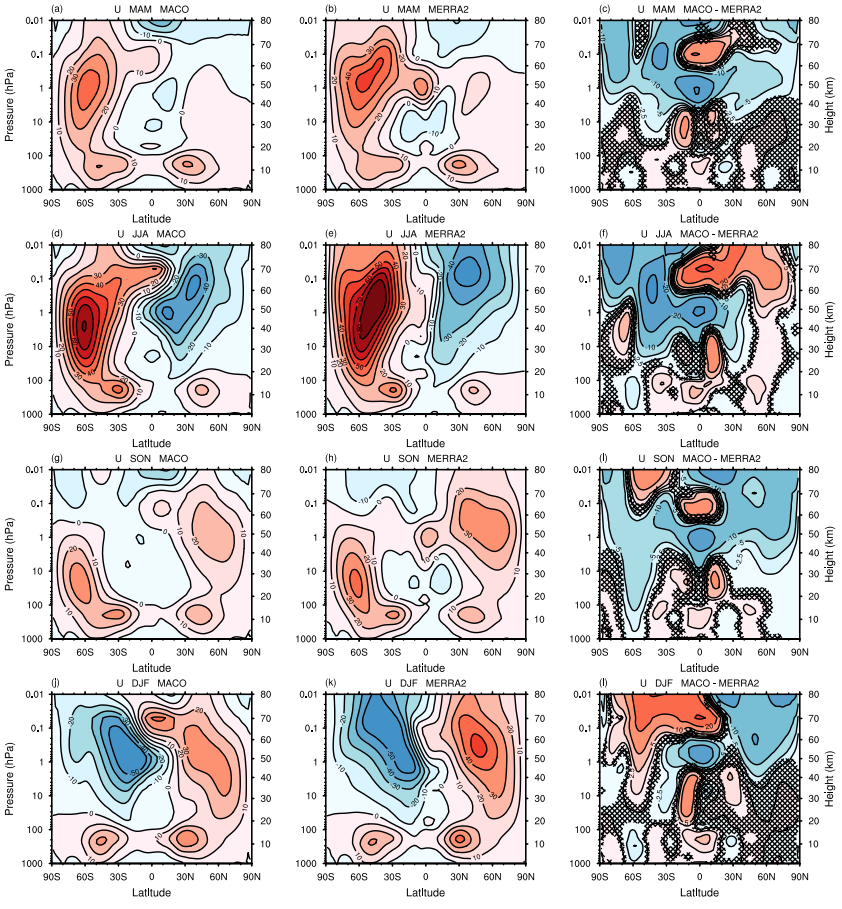

Figure 2. Latitude-altitude distributions of zonal wind simulated by the MACO (first column) from 1980 to 2014, zonal wind from the MERRA2 reanalysis data (second column), and the differences between the model and MERRA2 (third column) (units: m/s). Panels (a-c), (d-f), (g-i), and (j-l) show results for spring, summer, autumn, and winter, respectively. In the third column, contour intervals are -40, -20, -10, -5, -2.5, 0, 2.5, 5, 10, 20, and 40. The slanted grid areas denote regions where the zonal wind differences are not statistically significant at the 95% confidence level based on a t-test.

https://doi.org/10.5194/egusphere-2025-3636
Preprint. Discussion started: 8 August 2025

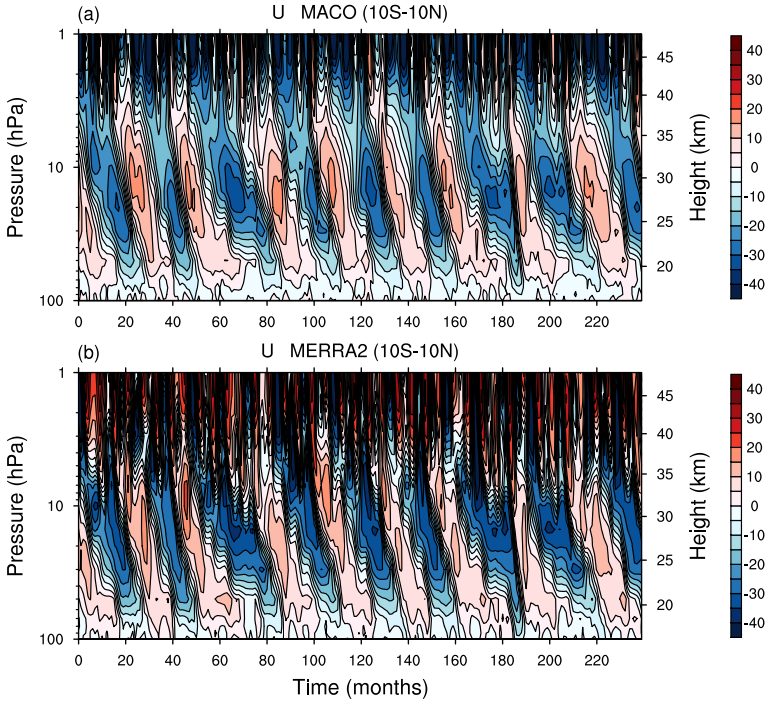

Figure 3. Monthly evolution of the 100-1 hPa tropical (10°S-10°N) averaged zonal wind from (a) MACO model simulation and (b) MERRA2 reanalysis data during 1995-2014 (units: m/s).

3.3 Evaluation of atmospheric chemistry

3.3.1 Climatology of trace gas

Methane (CH_4) is an important source of water vapor in the stratosphere and also a crucial tracer for stratospheric circulation. Figure 4 shows the latitude-height distribution of annual mean CH_4 volume mixing ratios and its comparison with observations. The model simulation (Fig. 4a) reproduces well the distribution of CH_4 seen in observations (Fig. 4b). The CH_4 mixing ratio contours bulge upwards in low-latitude regions and dip downwards in mid- and high-latitude regions, corresponding to

https://doi.org/10.5194/egusphere-2025-3636
Preprint. Discussion started: 8 August 2025

the ascending and descending branches of the Brewer-Dobson (B-D) circulation, respectively. The relatively flat contours observed in mid-latitudes, resulting from rapid atmospheric mixing due to planetary wave breaking, are also reasonably captured by the model. Performance of the model in simulating stratospheric CH_4 below 10 hPa is excellent, with deviations from observations within 5%. However, above 10 hPa, simulated CH_4 concentrations are higher than observed values, and the deviations increase with altitude, exceeding 50% in the lower mesosphere. The overestimation can be attributed to two main factors. For the overestimation in the middle and upper stratosphere, the height of the 0.8 ppmv contour over the equator is notably higher than that in observations, suggesting potentially excessive vertical transport in the model that leads to overestimated vertical transport of CH_4. The bias in the mesosphere may stem from neglect of the CH_4 photolysis at the Lyman-α line (121.567 nm) in the photolysis rate calculation, resulting in underestimation of the CH_4 photolysis rate. The combined effect of these two factors likely amplifies the bias in the mesosphere.

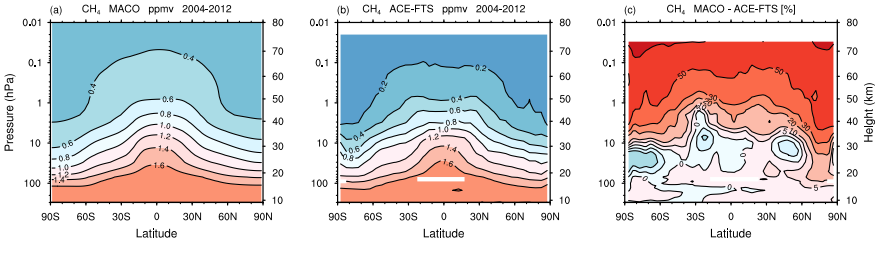

Figure 4. Latitude-altitude distributions of CH_4 volume mixing ratios (in ppmv) from (a) MACO model simulation and (b) ACE-FTS satellite observations during 2004-2012, as well as the relative differences between the model simulation and ACE-FTS satellite data (%).

Figure 5 presents the latitude-height distribution of annual mean N_2O volume

https://doi.org/10.5194/egusphere-2025-3636
Preprint. Discussion started: 8 August 2025

mixing ratios and its comparison with observations. The model also reproduces well the observed N_2O distribution. Similar to CH_4, the main differences for N_2O are primarily found in the middle and upper stratosphere, increasing with altitude. In the lower stratosphere, simulated N_2O concentrations are close to observations. In the middle stratosphere, the simulated results display hemispheric asymmetry, with smaller differences in the Northern Hemisphere but a negative bias compared to observations in the Southern Hemisphere, reaching a maximum over the Antarctic region. From the upper stratosphere upwards, simulated N_2O concentrations become higher than observed, and the bias increases rapidly with altitude.

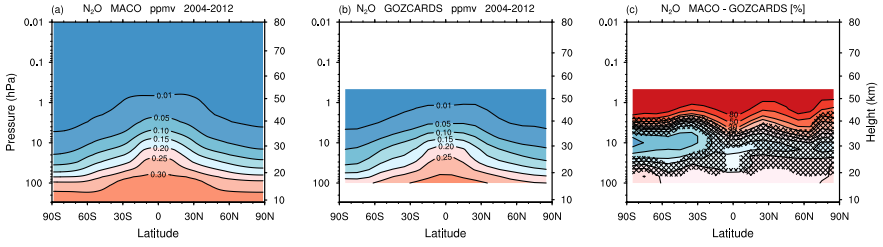

Figure 5. Latitude-altitude distributions of N_2O volume mixing ratios (in ppmv) from (a) MACO model simulation and (b) GOZCARDS data during 2004-2012, as well as the relative differences between the model simulation and GOZCARDS data (%). The slanted grid areas denote regions where the differences are not statistically significant at the 95% confidence level based on a t-test.

This overestimation of both CH_4 and N_2O in the mid-upper stratosphere and above is highly consistent with corresponding evaluation results for SOCOL4 reported by Sukhodolov et al. (2021). Since both MACO and SOCOL4 utilize the ECHAM6 as their atmospheric component, dynamical causes for biases in these chemical species

https://doi.org/10.5194/egusphere-2025-3636
Preprint. Discussion started: 8 August 2025

inherit primarily from ECHAM6 in both models. Regarding biases attributable to chemistry, analysis reveals that while the look-up table method used in SOCOL4 includes photolysis of CH_4 at the Lyman-α line, it still underestimates the photolysis rate at this line. Furthermore, the online photolysis scheme in MACO neglects CH_4 photolysis at the Lyman-α line. Both findings indicate that inaccurate calculation of photolysis rates contribute to the CH_4 simulation bias and also explain why the mesospheric bias in MACO is larger than in SOCOL4. The situation is similar for N_2O, where photolysis at shorter wavelengths is also underestimated.

Figure 6 presents the latitude-height distribution of the annual mean water vapor (H_2O) volume mixing ratio and its comparison with observations. The comparison between the water vapor distributions in Fig. 6a and b shows that the model successfully simulates the minima centers near the lowermost stratosphere over the Antarctic and the Equator. The Antarctic H_2O minimum is caused by dehydration via PSCs, indicating the model captures the state of PSCs reasonably well. Conversely, the model fails to reproduce the observed maximum center from the stratopause to the lower mesosphere. The difference distribution between the model and observations in Fig. 6c clearly shows that the model performs well in the stratosphere, with biases largely within 5%. However, between 1 and 0.1 hPa, the simulated H_2O concentrations are significantly lower than observations, with biases exceeding 10% in the middle and low latitudes, and the Antarctic. Tropospheric water vapor transport and methane oxidation from the stratosphere to the mesosphere are the two primary sources of H_2O in the middle atmosphere. Tropospheric transport contributes relatively little to H_2O at the stratopause

https://doi.org/10.5194/egusphere-2025-3636
Preprint. Discussion started: 8 August 2025

due to dehydration at the tropopause. Therefore, the most likely cause for the simulated H_2O underestimation is that the model underestimates CH_4 photolysis at Lyman-α line. Simulated H_2O above 0.1 hPa is higher than observations, likely because the model does not account for H_2O photolysis at Lyman-α line, resulting in reduced H_2O loss. As H_2O is an important radiative gas in the mesosphere, its underestimation may be a significant reason for the cold biases from the stratopause to the mesosphere in Figure 1.

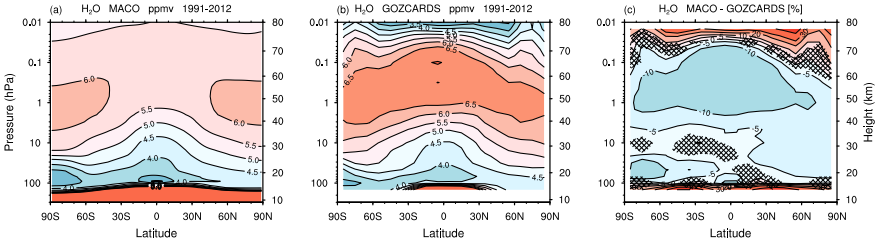

Figure 6. Latitude-altitude distributions of H_2O volume mixing ratios (in ppmv) from (a) MACO model simulation and (b) GOZCARDS data for the period 1991-2012, as well as the relative differences between the model simulation and GOZCARDS data (%). The slanted grid areas denote regions where the differences are not statistically significant at the 95% confidence level based on a t-test.

Figure 7 further displays the latitude-month variation of H_2O at 70 hPa compared with observations. The model simulates the global distribution and seasonal variations of H_2O well, and successfully reproduces the observed H_2O minima in the tropics during January-May and in the Antarctic during June-November. However, the simulated H_2O values exhibit a generally low bias, especially over the Antarctic from January to May, where concentrations are significantly lower than observed. This

https://doi.org/10.5194/egusphere-2025-3636
Preprint. Discussion started: 8 August 2025

indicates the simulation of PSC seasonal variations requires further improvement.

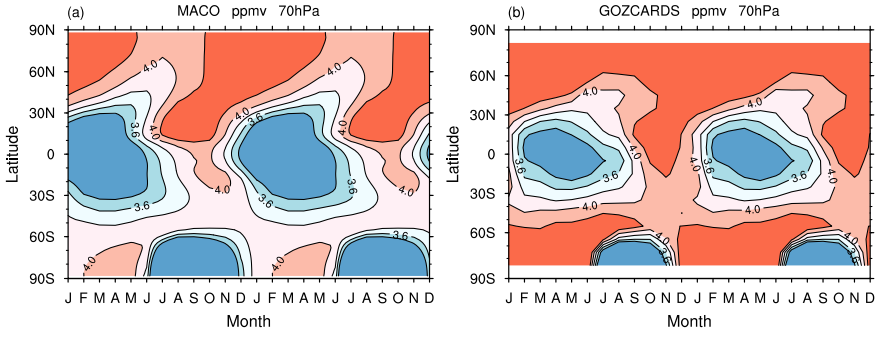

Figure 7. Month-latitude distributions of H_2O volume mixing ratios (in ppmv) at 70 hPa from (a) MACO model simulation and (b) GOZCARDS data for the years 1991-2012.

530

HNO_3 is an important reservoir for NO_x, influencing stratospheric NO_x concentrations and its catalytic cycles for ozone loss. It also plays a key role in polar heterogeneous chemistry. Figure 8 presents the latitude-height distribution of the annual mean HNO_3 volume mixing ratio and its comparison with observations. Overall, the 535 model reproduces the observed stratospheric distribution of HNO_3 and successfully simulates the locations of the maxima centers in both hemispheres. However, simulated HNO_3 concentrations are lower than observations throughout the stratosphere. In the lower to middle stratosphere, model biases are concentrated in the middle and low latitudes, exceeding 20% and being largest in the low latitudes. This underestimation 540 may relate to an overestimation of HNO_3 wet scavenging. In the upper stratosphere, model biases exceed 30% and are largest over the poles, likely linked to the underestimation of H_2O at these altitudes. Reduced H_2O leads to less OH production, thereby reducing HNO_3 formation.

https://doi.org/10.5194/egusphere-2025-3636
Preprint. Discussion started: 8 August 2025

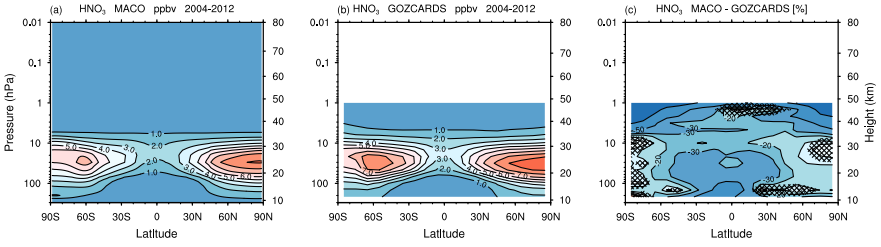

Figure 8. Latitude-altitude distributions of HNO_3 volume mixing ratios (in ppbv) from (a) MACO model simulations and (b) GOZCARDS data for the period 2004-2012, as well as the relative differences between the model simulation and GOZCARDS data (%). The slanted grid areas denote regions where the differences are not statistically significant at the 95% confidence level based on a t-test.

545

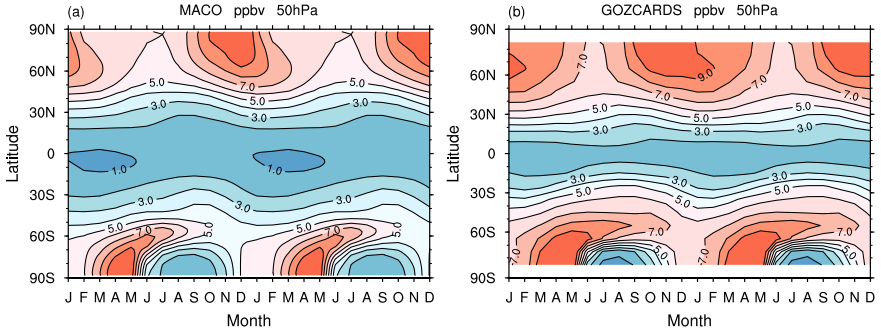

Figure 9. Month-latitude distributions of HNO_3 volume mixing ratios (in ppbv) at 50 hPa from (a) MACO model simulation and (b) GOZCARDS data for the years 2004-2012.

As HNO_3 is essential for forming PSCs, its accurate simulation is crucial for polar ozone chemistry. Figure 9 shows the latitude-month variation of HNO_3 at 50 hPa and its comparison with observations. The latitude distribution and seasonal variation of 550 HNO_3 generally correspond well with observations, with the Antarctic simulation performing particularly well. However, the simulated duration of sustained HNO_3 loss in both polar regions is longer than observed. This difference is especially pronounced

https://doi.org/10.5194/egusphere-2025-3636
Preprint. Discussion started: 8 August 2025

in the Arctic, where continuous loss persists from late winter through spring.

Figure 10 presents the latitude-height distribution of the annual mean hydrogen chloride (HCl) volume mixing ratio and its comparison with observations. HCl is a critically important chlorine reservoir and plays a significant role in polar ozone chemistry. The model reproduces the spatial distribution of HCl well, with the best performance for the middle to upper stratosphere. Specifically, except for the lowermost stratosphere over the poles and the lower stratosphere over the equator, the absolute bias in the stratosphere is mostly within 5%. In the equatorial lower stratosphere, the simulated HCl concentrations are higher than observations by more than 10%. In the lower stratosphere over both polar regions, simulated HCl concentrations are lower than observations by more than 10%, with the Antarctic exhibiting a more pronounced difference.

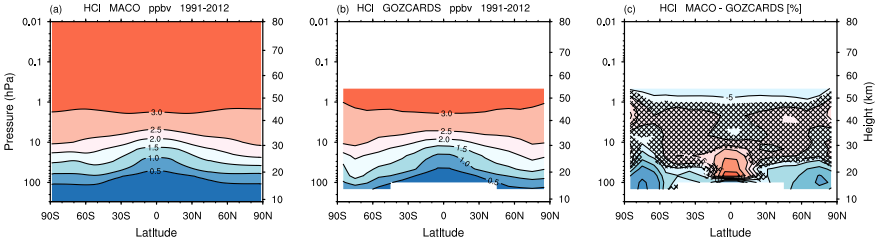

Figure 10. Latitude-altitude distributions of HCl volume mixing ratios (in ppbv) from (a) MACO model simulation and (b) GOZCARDS data for the period 1991-2012, as well as the relative differences between the model simulation and GOZCARDS data (%). The slanted grid areas denote regions where the differences are not statistically significant at the 95% confidence level based on a t-test.

https://doi.org/10.5194/egusphere-2025-3636
Preprint. Discussion started: 8 August 2025

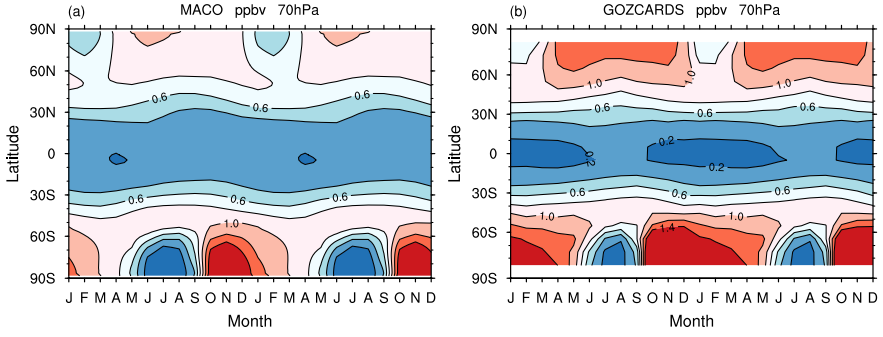

Figure 11. Month-latitude distributions of HCl volume mixing ratios (in ppbv) at 70 hPa from (a) MACO model simulation and (b) GOZCARDS data for the years 1991-2012.

Furthermore, Figure 11 shows the latitude-month variation of HCl at 70 hPa and its comparison with observations. The model captures the seasonal variations of HCl in both polar regions reasonably well compared to observations, successfully simulating the wintertime decrease in HCl due to PSC formation. However, simulated HCl concentrations from summer to fall are significantly lower than observed in both polar regions, with the Arctic exhibiting consistently lower concentrations throughout the year. Synthesizing results for HNO_3, H_2O, and HCl reveals that the underestimation of HCl in the polar regions is similar to the behavior of HNO_3 and H_2O. This collectively indicates the model overestimates PSCs, leading to enhanced uptake of HNO_3, H_2O, and HCl into PSCs. This PSC overestimation may relate to the simulated cold bias in the lower to middle stratosphere. A closer analysis of Figure 1 shows that temperatures in the lower to middle stratosphere over the Arctic are lower than observed in almost all seasons (Fig. 1c, f, i, l). These lower temperatures favor PSC formation, thereby promoting gas-phase HCl depletion. Similarly, a cold bias is also found in the Antarctic

https://doi.org/10.5194/egusphere-2025-3636
Preprint. Discussion started: 8 August 2025

lower stratosphere during summer (Fig. 1l) and fall (Fig. 1c), which corresponds well with that the simulated HCl underestimation in the Antarctic occurs primarily during summer and fall.

Figure 12 presents the latitude-height distribution of the annual mean ozone (O_3) volume mixing ratio and its comparison with observations. Comparison of Figure 12a and b shows the model successfully reproduces the spatial distribution of ozone and accurately simulates the location of the stratospheric ozone maximum center. However, significant concentration biases remain between the model and observations. Specifically, except for the middle and high latitudes of the Northern Hemisphere, simulated ozone concentrations in the lower stratosphere are more than 10% higher than observations, with the bias increasing closer to the tropopause. Two bias maxima exist over the equator and in the Southern Hemisphere mid-latitudes (Fig. 12c). The model overestimation of lower stratospheric ozone concentrations is a phenomenon common to most chemistry-climate models. Significant uncertainty and disagreement remain regarding the causes of this overestimation (Eyring et al., 2006; Morgenstern et al., 2009; Froidevaux et al., 2019; Archibald et al., 2020; Sukhodolov et al., 2021; Keeble et al., 2021). For MACO, one possible reason for the overestimation might be an overestimation of the O_2 photolysis rate. The evaluation of the Fast-JX photolysis rates by Sukhodolov et al. (2016) shows that at 20-30 km, O_2 photolysis rates calculated by Fast-JX can be up to 20% higher than those computed by line-by-line integration, which would increase ozone production. It is important to note that, due to the complex interactions between the lower stratosphere and troposphere (Holton et al., 1995),

https://doi.org/10.5194/egusphere-2025-3636
Preprint. Discussion started: 8 August 2025

identifying the specific causes for this overestimation is difficult and requires more targeted in-depth analysis.

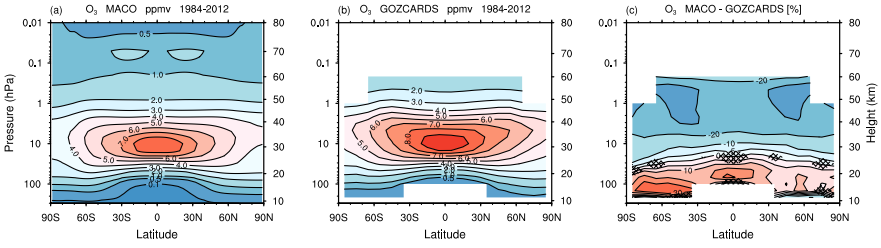

Figure 12. Latitude-altitude distributions of O_3 volume mixing ratios (in ppmv) from (a) MACO model simulation and (b) GOZCARDS data for the period 1984-2012, as well as the relative differences between the model simulation and GOZCARDS data (%). The slanted grid areas denote regions where the differences are not statistically significant at the 95% confidence level based on a t-test.

From the middle stratosphere upwards to the lower mesosphere, the simulated ozone concentrations are more than 20% lower than observations, and the largest biases occur near the stratopause in the mid-latitudes (Fig. 12c). Similar results have been found in evaluations of the UKCA CCM (Morgenstern et al., 2009; Archibald et al., 2020). The SOCOL4 model, however, shows better agreement in the tropical upper stratosphere, with underestimation persisting at mid-latitudes (Sukhodolov et al., 2021). Sukhodolov et al. (2016) highlighted that accurately calculating the O_2 photolysis rate in the upper stratosphere and mesosphere is crucial for ozone production. One reason for the better performance of SOCOL4 in the tropical upper stratosphere is its correction of the O_2 photolysis rate in the 10-1 hPa region by a factor of 1.2. While both our model and UKCA use the online photolysis schemes from the Fast-J family, evaluations reveal

https://doi.org/10.5194/egusphere-2025-3636
Preprint. Discussion started: 8 August 2025

biases in the upper stratosphere and especially the mesosphere compared to line-by-line integration results. These results suggest that the underestimation of ozone in the tropical middle and upper stratosphere in MACO might stem from neglecting the calculation of O_2 photolysis rates below 177 nm (e.g., at Lyman-α line). For the mid- and high-latitudes, Sukhodolov et al. (2021) noted that the underestimation in the upper stratosphere has been present since the first version of the SOCOL model. They attributed this to the insufficient vertical resolution of ECHAM6 affecting wave propagation and breaking in the middle atmosphere, ultimately leading to reduced ozone through a weakened polar vortex and meridional transport gradients. Since MACO also uses ECHAM6 as its atmospheric component, it may suffer from this same issue. Indeed, the ECHAM6 versions used by SOCOL4 and MACO, along with the UKCA model used by Archibald et al. (2020), all have fewer vertical layers in the middle atmosphere compared to the troposphere. This commonality likely explains why similar results appear in evaluations of these models. The above analysis indicates that accurate photolysis rate calculations are crucial for simulating ozone in the tropical upper stratosphere, whereas dynamical processes likely play a more significant role than photolysis alone in extra-tropical regions.

https://doi.org/10.5194/egusphere-2025-3636
Preprint. Discussion started: 8 August 2025

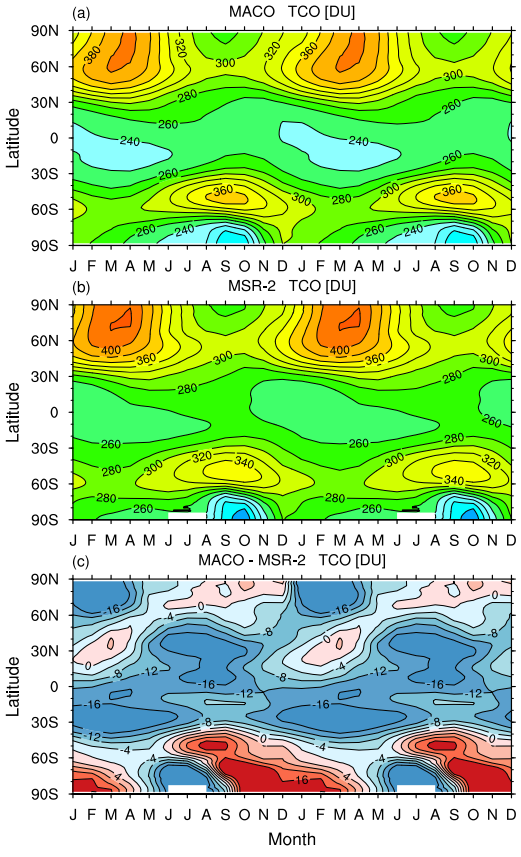

Figure 13. Month-latitude distributions of total column ozone from (a) MACO model simulation and (b) MSR2 reanalysis data for the years 1980-2014, as well as (c) the differences between the model simulation and MSR2 data (units: DU).

Figure 13 presents the latitude-month distribution of total column ozone (TCO) and its comparison with the MSR2 reanalysis data. The model successfully reproduces the spatio-temporal distribution of TCO and reasonably simulates the Antarctic ozone hole. Analysis of the differences between model and observation reveals that simulated TCO is lower than observed throughout the year in the tropics. This is likely due to the underestimation of the ozone maximum near 10 hPa and ozone concentrations above

https://doi.org/10.5194/egusphere-2025-3636
Preprint. Discussion started: 8 August 2025

10 hPa by the model (Fig. 12c). In the mid-latitudes of the Northern Hemisphere, model results show underestimation primarily in summer. Over the Arctic, simulated winter TCO is more than 16 Dobson Units (DU) lower than observations, consistent with the ozone underestimation in the upper stratosphere seen in Figure 12. Simulated Southern Hemisphere mid-latitude TCO is lower than observed in winter and spring and higher in summer and fall. Over the Antarctic, simulated TCO is lower than observed in summer but higher in spring, fall, and winter, with a maximum positive bias exceeding 16 DU. This pattern might relate to the simulated polar heterogeneous chemistry processes. It is noteworthy that the MSR2 reanalysis data also exhibit large uncertainties over the polar regions. Therefore, definitive attribution of causes requires more reliable observational datasets for comparison and analysis.

3.3.2 Evaluation of ozone evolution

Figure 14 presents the temporal evolution of TCO for five latitude bands and a near-global average. For the polar regions of the Southern and Northern Hemispheres, this study only considers TCO changes for October and March, respectively, as these months typically correspond to the ozone depletion period during the end of winter to the beginning of spring. For other latitude bands, the annual mean TCO is calculated. Figure 14a shows the evolution of Antarctic TCO in October. The model successfully captures the decreasing trend in ozone from 1980 to 1995. Simultaneously, owing to the entry into force of the Montreal Protocol, emissions of ozone-depleting substances stabilized around 2000. The model reasonably reproduces the subsequent gradual increase and stabilization of ozone after 2000. Figure 14b displays the results for the

https://doi.org/10.5194/egusphere-2025-3636
Preprint. Discussion started: 8 August 2025

Arctic in March. The model also reproduces the trends from 1980 to 1995, particularly the ozone decline during the 1990s. However, the model shows deviations in simulating the post-2000 ozone trend, likely related to the strong influence of dynamical processes in the Arctic. Figure 14c shows the results for Southern Hemisphere mid-latitudes. The model successfully reproduces the ozone evolution trend, showing minor bias compared to observations. In the Northern Hemisphere mid-latitudes (Fig. 14d), the model also performs reasonably well in simulating ozone changes, although the ozone content is generally lower than observations, consistent with the findings in Figure 13c. Figure 14e and f present the ozone evolution for the tropics and near-global average, respectively. The model successfully reproduces the observed evolution trends and variability characteristics. However, both results also indicate that the ozone content is generally lower than observations, as previously noted in Figure 13c.

https://doi.org/10.5194/egusphere-2025-3636
Preprint. Discussion started: 8 August 2025

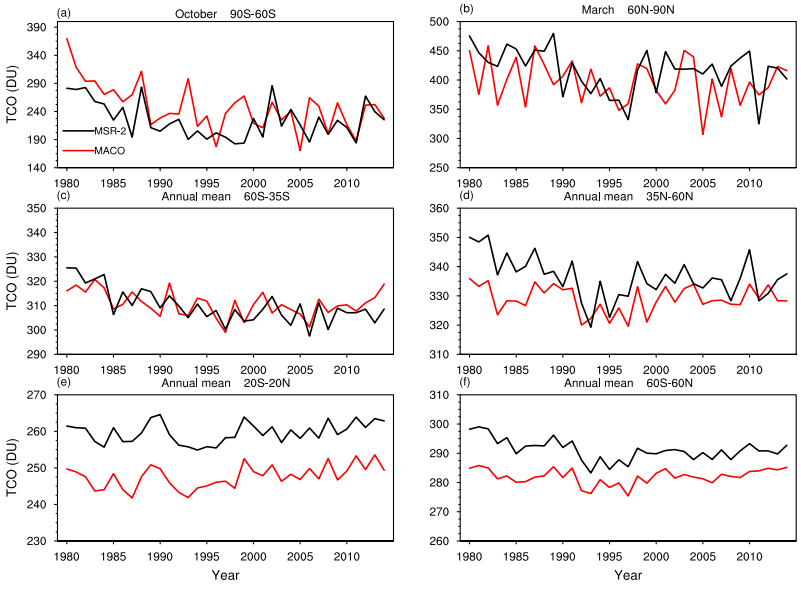

Figure 14. Time series of averaged total column ozone (units: DU) for (a) 90°S-60°S, (b) 60°N-90°N, (c) 60°S-35°S, (d) 35°N-60°N, (e) 20°S-20°N, and (f) 60°S-60°N, covering the period 1980-2014. Results for October, March, and annual averages are shown for (a, b) and (c-f), respectively. Red lines denote MACO model simulation, while black lines denote MSR2 data.

695 To deepen understanding of the relationships between stratospheric ozone, temperature, and chlorine loading, Figure 15 further shows the evolution of ozone, temperature, and HCl in the Antarctic stratosphere. For the upper stratosphere (Fig. 15a), simulated ozone exhibits relatively stable temporal variations consistent with observations, though with lower concentration. Correspondingly, simulated upper 700 stratospheric temperatures are close to observations, but exhibit larger interannual variability (Fig. 15c). As seen in Figure 15e, the model accurately reproduces the historical changes in upper stratospheric HCl, successfully capturing the feature where

https://doi.org/10.5194/egusphere-2025-3636
Preprint. Discussion started: 8 August 2025

chlorine loading peaked around 1995-2000 before beginning a slow decline. Analysis of the lower stratosphere shows the model successfully simulates the persistent ozone depletion trend before 1995. However, it underestimates the magnitude of the brief increase in ozone content around 2000-2005 (Fig. 15b). The simulated lower stratospheric temperature trend shares some similarity with observations but still exhibits considerable uncertainty (Fig. 15d). The historical variation of HCl shown in Figure 15f indicates the model values are closer to observations around 1990-2000, but are lower thereafter.

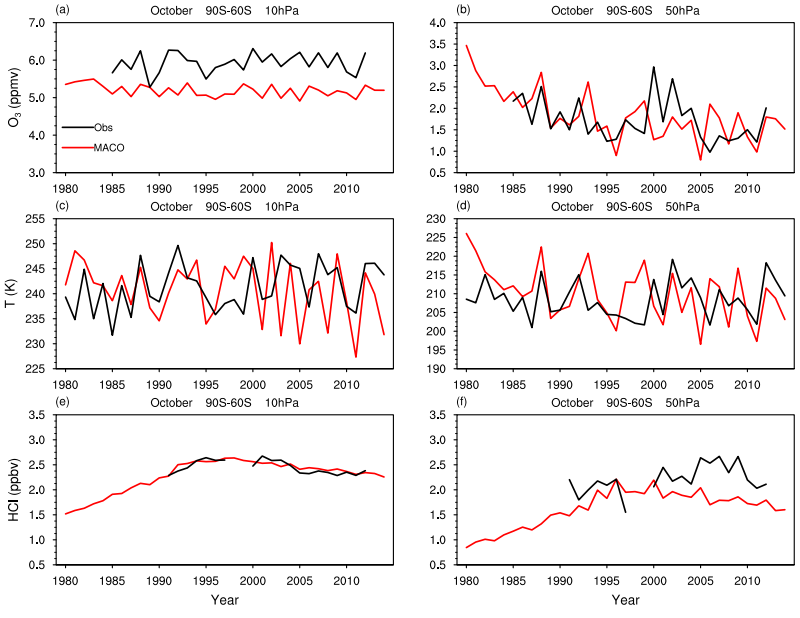

Figure 15. Time series of (a, b) O_3 (in ppmv), (c, d) temperature (in K), and (e, f) HCl (in ppbv) for 90°S-60°S average, at 10 hPa (first column) and 50 hPa (second column) for October from 1980 to 2014. Red lines denote MACO model simulation, while black lines denote observational data, with O_3 and HCl observations from GOZCARDS and temperature observations from MERRA2.

https://doi.org/10.5194/egusphere-2025-3636
Preprint. Discussion started: 8 August 2025

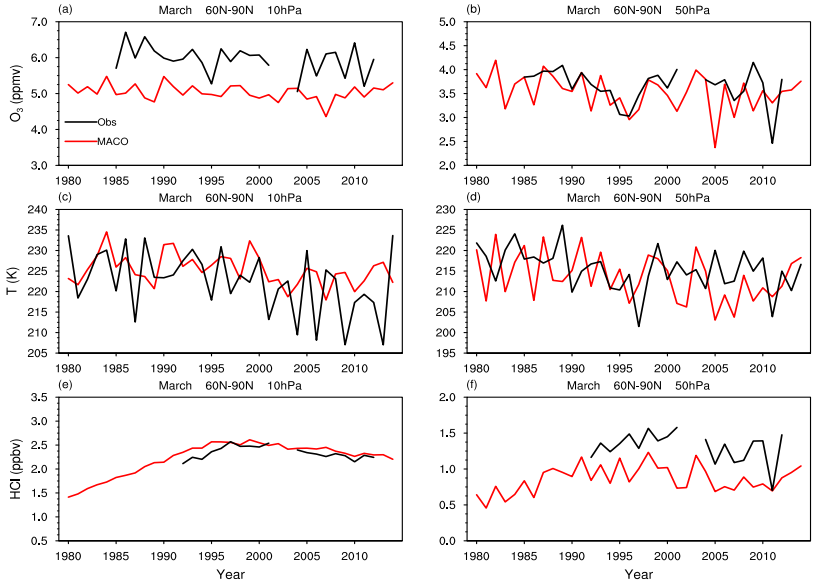

Figure 16. Time series of (a, b) O_3 (in ppmv), (c, d) temperature (in K), and (e, f) HCl (in ppbv) for 60°N-90°N average, at 10 hPa (first column) and 50 hPa (second column) for March from 1980 to 2014. Red lines denote MACO model simulation, and black lines denote observational data, with O_3 and HCl observations from GOZCARDS and temperature observations from MERRA2.

715 Figure 16 presents the evolution of ozone, temperature, and HCl in the Arctic stratosphere. Simulated upper stratospheric ozone is also lower than observed (Fig. 16a), but the model correctly captures the relatively stable concentration throughout the simulation period. The model reasonably captures the decreasing trend in upper stratospheric temperature after 2000, but exhibits large differences in interannual 720 variability compared to observations (Fig. 16c). Results in Figure 16e again demonstrate the model accurately reflects the historical evolution of upper stratospheric HCl content. For the lower stratosphere, the simulated ozone trend before 2000 agrees

https://doi.org/10.5194/egusphere-2025-3636
Preprint. Discussion started: 8 August 2025

reasonably well with observations, but significant deviations appear after 2000. Notably, the model simulates significant depletion in 2005, whereas the depletion is observed in 2011 in the dataset (Fig. 16b). Additionally, biases exist in the simulation of lower stratospheric temperature, showing substantially different interannual variability compared to observations (Fig. 16d). Simulated lower stratospheric HCl content is lower than observations, similar to the Antarctic results.

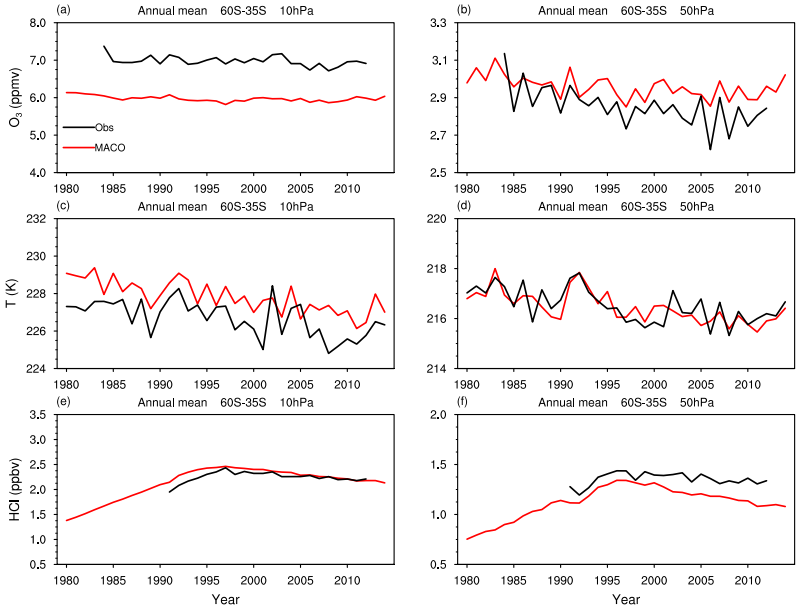

Figure 17. Annual time series of (a, b) O_3 (in ppmv), (c, d) temperature (in K), and (e, f) HCl (in ppbv) for 60°S-35°S average, at 10 hPa (first column) and 50 hPa (second column) from 1980 to 2014. Red lines denote MACO model outputs, while black lines denote observational data, with O_3 and HCl observations from GOZCARDS, and temperature observations from MERRA2.

Figure 17 displays the evolution of ozone, temperature, and HCl in the Southern Hemisphere mid-latitude stratosphere. The model reproduces the evolution reasonably

https://doi.org/10.5194/egusphere-2025-3636
Preprint. Discussion started: 8 August 2025

well for both the upper and lower stratospheric ozone, although biases exist in absolute values (Fig. 17a and b). The model also effectively captures the observed cooling trend in stratospheric temperature, with the lower stratospheric results showing the closest agreement (Fig. 17c and d). Results in Figure 17e show the model accurately reproduces the temporal evolution of HCl and the simulated post-peak decline rate closely matches observations. For lower stratospheric HCl (Fig. 17f), the model simulates a decline rate somewhat faster than observed.

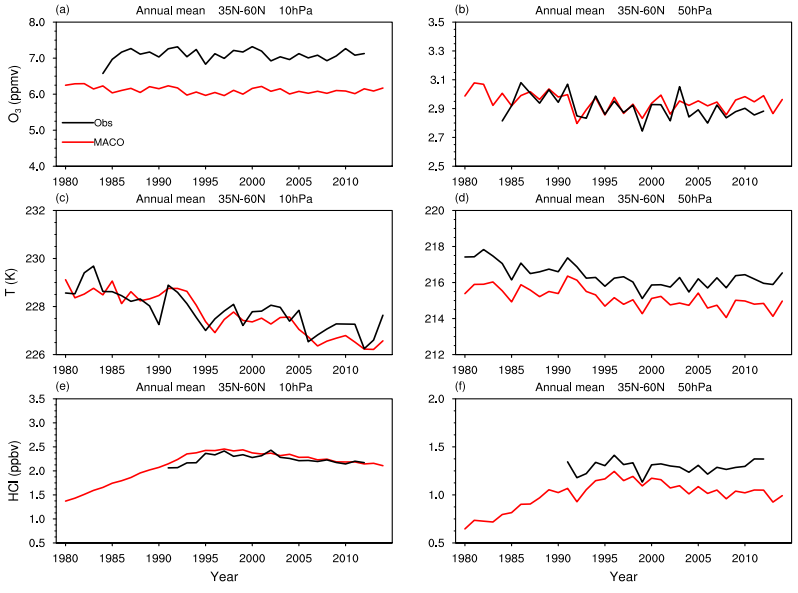

Figure 18. Annual time series of (a, b) O_3 (in ppmv), (c, d) temperature (in K), and (e, f) HCl (in ppbv) for 35°N-60°N average, at 10 hPa (first column) and 50 hPa (second column) from 1980 to 2014. Red lines denote MACO model simulation, and black lines denote observational data, with O_3 and HCl observations from GOZCARDS, and temperature observations from MERRA2.

Figure 18 shows the evolution of ozone, temperature, and HCl in the Northern

https://doi.org/10.5194/egusphere-2025-3636
Preprint. Discussion started: 8 August 2025

Hemisphere mid-latitude stratosphere. Overall, the model successfully captures the historical trends of ozone, temperature, and HCl. Simulation of lower stratospheric ozone, upper stratospheric temperature, and upper stratospheric HCl shows the closest agreement with observations (Fig. 18b, c, and e). Conversely, simulated upper stratospheric ozone, lower stratospheric temperature, and lower stratospheric HCl are lower than observed.

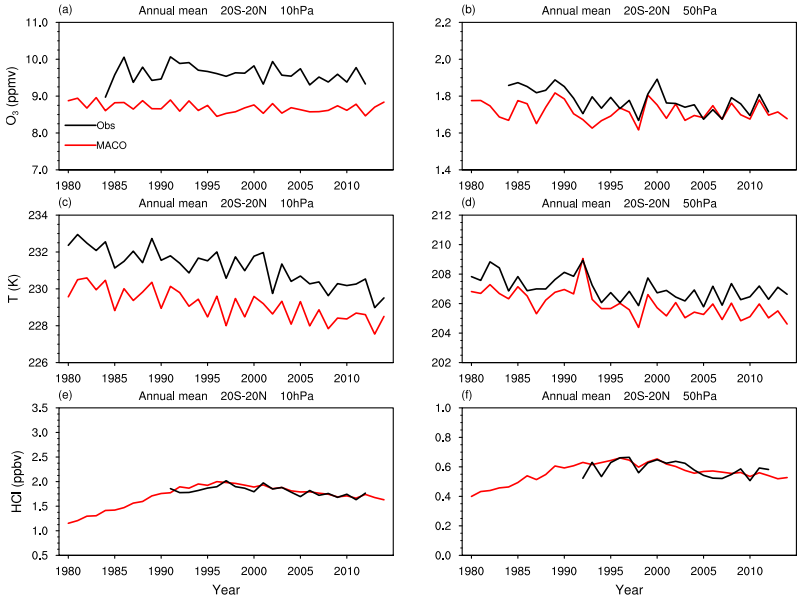

Figure 19. Annual time series of (a, b) O_3 (in ppmv), (c, d) temperature (in K), and (e, f) HCl (in ppbv) for 20°S-20°N average, at 10 hPa (first column) and 50 hPa (second column) from 1980 to 2014. Red lines denote MACO model simulation, and black lines denote observational data, with O_3 and HCl observations from GOZCARDS, and temperature observations from MERRA2.

Figure 19 presents the evolution of ozone, temperature, and HCl in the tropical stratosphere. Results are generally close to observations, except for lower values in

https://doi.org/10.5194/egusphere-2025-3636
Preprint. Discussion started: 8 August 2025

upper stratospheric ozone and temperature (Fig. 19a and c). The model performs well in simulating the trends of ozone, temperature, and HCl.

Synthesizing the results from Figures 15 to 19 reveals that the model performs well in simulating trends and variability of ozone, temperature, and HCl in low and mid-latitudes, particularly excelling in simulating upper stratospheric HCl. Significant uncertainties remain in simulating the polar regions, which may also relate to the relatively larger uncertainties in polar observational data. Furthermore, consistent with the analyses in Figures 12 and 10, the model simulates systematically lower ozone in the upper stratosphere and lower HCl in the lower stratosphere of mid-to-high latitudes compared to observations. Regarding temperature biases at 50 hPa in mid-to-high latitudes, owing to the complex interactions between the lower stratosphere and troposphere, investigating the sources of lower stratospheric temperature biases requires sophisticated diagnostic tools and multiple sensitivity studies. This represents a substantial target for future research.

4 Summary and Outlook

This study has introduced the new chemistry-climate model MACO and provided a comprehensive evaluation of its performance in simulating the middle atmosphere from 1980 to 2014. The analysis reveals that MACO is a capable tool for studying chemistry-climate interactions, while also highlighting specific areas where targeted improvements are needed.

MACO demonstrates robust capabilities in simulating key dynamical and chemical processes in the middle atmosphere. Specifically, the simulated tropospheric

https://doi.org/10.5194/egusphere-2025-3636
Preprint. Discussion started: 8 August 2025

and lower stratospheric temperatures and zonal winds agree well with observations. The model also provides a generally reasonable simulation of the climatological distributions of major stratospheric chemical constituents, including CH_4, N_2O, H_2O, HNO_3, HCl, and O_3. Analysis indicates that MACO simulates transport and chemical processes of key stratospheric constituents well. Furthermore, the model effectively captures the annual cycle of the Antarctic ozone hole and Arctic ozone depletion. Evaluation of TCO time series reveals that MACO successfully reproduces the decreasing Antarctic TCO trend from 1980 to 1995 and its subsequent gradual recovery after 2000. Further analysis indicates that MACO provides a realistic simulation of the historical evolution of stratospheric ozone, temperature, and HCl.

Nevertheless, MACO simulations exhibit several significant biases, most prominently within the upper stratosphere and mesosphere. The evaluation of MACO reveals an instructive interaction between biases originating from the model's dynamical core and those from its chemical scheme. The most significant dynamical bias than observed is the weaker polar vortex and the associated warm bias at the winter polar stratopause. This bias is a direct consequence of the model's moderate vertical resolution (L47), which is insufficient to fully resolve the planetary wave forcing that drives the stratospheric circulation. This fundamental dynamical bias subsequently influences the transport of chemical species.

Separately, biases originating from the chemical scheme itself are also evident. The omission of photolysis at wavelengths below 177 nm is the dominant factor for the overestimation of CH_4 and N_2O and underestimation of tropical O_3 in the upper

https://doi.org/10.5194/egusphere-2025-3636
Preprint. Discussion started: 8 August 2025

stratosphere and mesosphere. In mid-high latitudes, the insufficient vertical resolution likely plays a more critical role than photolysis rate bias in driving the substantial O_3 underestimation. The overestimation of CH_4, in turn, leads to an underestimation of H_2O, which subsequently contributes to a cold temperature bias near the stratopause outside polar regions. These findings underscore that improving model fidelity requires a dual-pronged approach that addresses both the underlying dynamical framework and the specifics of the chemical process representations.

It is crucial to recognize that the biases identified in MACO are not unique. The weak vortex/warm pole bias is a well-documented issue in many GCMs, particularly those run at similar resolutions. Likewise, the positive bias in lower stratospheric ozone is a notoriously difficult problem faced by the entire CCM community, with its roots in the complex interaction of transport, chemistry, and dynamical variability. The fact that MACO, which uses the ECHAM6 dynamical core, exhibits biases similar to other ECHAM-based models like SOCOL is not a weakness of this study. Rather, it validates MACO as a representative model of its class and establishes it as a valuable tool for participating in community-wide efforts to understand and resolve these persistent challenges.

Based on the diagnostic evaluation presented here, we have identified several prioritized pathways for future model development. First, increase vertical resolution. The most critical step to improve the simulation of stratospheric dynamics is to increase the vertical resolution. Future work should involve sensitivity experiments with a higher-resolution version of the model (e.g., using the L95 configuration of ECHAM6)

https://doi.org/10.5194/egusphere-2025-3636
Preprint. Discussion started: 8 August 2025

to quantify the impact on the polar vortex, temperature biases, and chemical transport. Second, refine the photolysis scheme. To address the significant biases in upper stratospheric and mesospheric chemistry, the implementation of photolysis calculations for wavelengths below 177 nm (e.g., Lyman-α line) is essential. This will directly impact the simulation of O_3, CH_4, N_2O, and H_2O.

In conclusion, MACO provides a solid foundation for future research. The work presented here not only characterizes the model's current capabilities but also lays out a roadmap for its continued development. By addressing the identified issues, future versions of MACO will become an even more powerful tool for advancing our understanding of the middle atmosphere and its role in the Earth system.

Code and data availability. The MACO code and simulation data are available at https://doi.org/10.5281/zenodo.16452132 (Zhu, 2025). MERRA-2 data are available at https://doi.org/10.5067/WWQSXQ8IVFW8 (Gelaro et al., 2017), managed by the NASA Goddard Earth Sciences (GES) Data and Information Services Center (DISC) (GMAO, 2015). GOZCARDS data can be obtained from https://disc.gsfc.nasa.gov/datasets?keywords=gozcards&page=1 (Froidevaux et al., 2015). ACE-FTS data can be downloaded from https://databace.scisat.ca/climatology/climatology_3.5.php (Bernath et al., 2005). MSRv2 data can be found at https://doi.org/10.21944/temis-ozone-msr2 (van der A et al., 2015).

https://doi.org/10.5194/egusphere-2025-3636
Preprint. Discussion started: 8 August 2025

Author contributions. LZ and ZX led the project. ZZ developed the model code, performed the model simulations, analyzed the data, and wrote the first draft. All authors contributed to the discussion and improvement of the paper.

Competing interests. The authors declare that they have no conflict of interest.

Financial support. This work was funded by the National Natural Science Foundation of China (Grant Nos. 42394123, 42271027, and 41971020), and the Strategic Priority Research Program of CAS (Grant No. XBD 41000000). ZZ acknowledges the support from the Fundamental Research Funds of the Institute of Atmospheric Physics, Chinese Academy of Sciences (E468081801).

References:

Archibald, A. T., O'Connor, F. M., Abraham, N. L., Archer-Nicholls, S., Chipperfield, M. P., Dalvi, M., Folberth, G. A., Dennison, F., Dhomse, S. S., Griffiths, P. T., Hardacre, C., Hewitt, A. J., Hill, R. S., Johnson, C. E., Keeble, J., Kohler, M. O., Morgenstern, O., Mulcahy, J. P., Ordonez, C., Pope, R. J., Rumbold, S. T., Russo, M. R., Savage, N. H., Sellar, A., Stringer, M., Turnock, S. T., Wild, O., and Zeng, G.: Description and Evaluation of the UKCA Stratosphere-Troposphere Chemistry Scheme (StratTrop Vn 1.0) Implemented in UKESM1, Geosci. Model Dev., 13, 1223-1266, https://doi.org/10.5194/gmd-13-1223-2020, 2020.

Austin, J.: A Three-Dimensional Coupled Chemistry-Climate Model Simulation of Past

https://doi.org/10.5194/egusphere-2025-3636
Preprint. Discussion started: 8 August 2025

Stratospheric Trends, J. Atmos. Sci., 59, 218-232, https://doi.org/10.1175/1520-0469(2002)059<0218:ATDCCC>2.0.CO;2, 2002.

Bernath, P. F., McElroy, C. T., Abrams, M. C., Boone, C. D., Butler, M., Camy-Peyret, C., Carleer, M., Clerbaux, C., Coheur, P. F., Colin, R., DeCola, P., DeMazière, M., Drummond, J. R., Dufour, D., Evans, W. F. J., Fast, H., Fussen, D., Gilbert, K., Jennings, D. E., Llewellyn, E. J., Lowe, R. P., Mahieu, E., McConnell, J. C., McHugh, M., McLeod, S. D., Michaud, R., Midwinter, C., Nassar, R., Nichitiu, F., Nowlan, C., Rinsland, C. P., Rochon, Y. J., Rowlands, N., Semeniuk, K., Simon, P., Skelton, R., Sloan, J. J., Soucy, M. A., Strong, K., Tremblay, P., Turnbull, D., Walker, K. A., Walkty, I., Wardle, D. A., Wehrle, V., Zander, R., and Zou, J.: Atmospheric Chemistry Experiment (ACE): Mission Overview, Geophys. Res. Lett., 32, https://doi.org/https://doi.org/10.1029/2005GL022386, 2005.

Bian, H. S. and Prather, M. J.: Fast-J2: Accurate Simulation of Stratospheric Photolysis in Global Chemical Models, J. Atmos. Chem., 41, 281-296, https://doi.org/10.1023/A:1014980619462, 2002.

Brasseur, G. P., Hauglustaine, D. A., Walters, S., Rasch, P. J., Muller, J. F., Granier, C., and Tie, X. X.: MOZART, a Global Chemical Transport Model for Ozone and Related Chemical Tracers 1. Model Description, J. Geophys. Res.-Atmos., 103, 28265-28289, https://doi.org/10.1029/98JD02397, 1998.

Brinkop, S. and Roeckner, E.: Sensitivity of a General Circulation Model to Parameterizations of Cloud-Turbulence Interactions in the Atmospheric Boundary Layer, Tellus, Series a (Dynamic Meteorology and Oceanography), 47A, 197-220, https://doi.org/10.1034/j.1600-0870.1995.t01-1-00004.x, 1995.

https://doi.org/10.5194/egusphere-2025-3636
Preprint. Discussion started: 8 August 2025

Brovkin, V., Boysen, L., Raddatz, T., Gayler, V., Loew, A., and Claussen, M.: Evaluation of Vegetation Cover and Land-Surface Albedo in MPI-ESM CMIP5 Simulations, J. Adv. Model. Earth Syst., 5, 48-57, https://doi.org/https://doi.org/10.1029/2012MS000169, 2013.

Buchholz, J.: Simulations of Physics and Chemistry of Polar Stratospheric Clouds with a General Circulation Model, phd, Johannes Gutenberg University of Mainz, Mainz, 2005.

Burkholder, J. B., Sander, S. P., Abbatt, J. P. D., Barker, J. R., Cappa, C., Crounse, J. D., Dibble, T. S., Huie, R. E., Kolb, C. E., Kurylo, M. J., Orkin, V. L., Percival, C. J., Wilmouth, D. M., and Wine, P. H.: Chemical Kinetics and Photochemical Data for Use in Atmospheric Studies, Evaluation Number 19, JPL Publication 19-5, Jet Propulsion Laborary, Pasadena, 2019.

Carslaw, K. S., Luo, B., and Peter, T.: An Analytic Expression for the Composition of Aqueous HNO3-H2so4 Stratospheric Aerosols Including Gas Phase Removal of HNO3, Geophys. Res. Lett., 22, 1877-1880, https://doi.org/10.1029/95GL01668, 1995.

Carslaw, K. S., Peter, T., and Clegg, S. L.: Modeling the Composition of Liquid Stratospheric Aerosols, Rev. Geophys., 35, 125-154, https://doi.org/10.1029/97RG00078, 1997.

Eastham, S. D., Weisenstein, D. K., and Barrett, S. R. H.: Development and Evaluation of the Unified Tropospheric-Stratospheric Chemistry Extension (UCX) for the Global Chemistry-Transport Model GEOS-Chem, Atmos. Environ., 89, 52-63, https://doi.org/10.1016/j.atmosenv.2014.02.001, 2014.

Eyring, V., Bony, S., Meehl, G. A., Senior, C. A., Stevens, B., Stouffer, R. J., and Taylor, K. E.: Overview of the Coupled Model Intercomparison Project Phase 6 (CMIP6) Experimental Design and Organization, Geosci. Model Dev., 9, 1937-1958, https://doi.org/10.5194/gmd-9-1937-2016, 2016.

https://doi.org/10.5194/egusphere-2025-3636
Preprint. Discussion started: 8 August 2025

Eyring, V., Butchart, N., Waugh, D. W., Akiyoshi, H., Austin, J., Bekki, S., Bodeker, G. E., Boville, B. A., Bruhl, C., Chipperfield, M. P., Cordero, E., Dameris, M., Deushi, M., Fioletov, V. E., Frith, S. M., Garcia, R. R., Gettelman, A., Giorgetta, M. A., Grewe, V., Jourdain, L., Kinnison, D. E., Mancini, E., Manzini, E., Marchand, M., Marsh, D. R., Nagashima, T., Newman, P. A., Nielsen, J. E., Pawson, S., Pitari, G., Plummer, D. A., Rozanov, E., Schraner, M., Shepherd, T. G., Shibata, K., Stolarski, R. S., Struthers, H., Tian, W., and Yoshiki, M.: Assessment of Temperature, Trace Species, and Ozone in Chemistry-Climate Model Simulations of the Recent Past, J. Geophys. Res.-Atmos., 111, https://doi.org/10.1029/2006JD007327, 2006.

Eyring, V., Cionni, I., Bodeker, G. E., Charlton-Perez, A. J., Kinnison, D. E., Scinocca, J. F., Waugh, D. W., Akiyoshi, H., Bekki, S., Chipperfield, M. P., Dameris, M., Dhomse, S., Frith, S. M., Garny, H., Gettelman, A., Kubin, A., Langematz, U., Mancini, E., Marchand, M., Nakamura, T., Oman, L. D., Pawson, S., Pitari, G., Plummer, D. A., Rozanov, E., Shepherd, T. G., Shibata, K., Tian, W., Braesicke, P., Hardiman, S. C., Lamarque, J. F., Morgenstern, O., Pyle, J. A., Smale, D., and Yamashita, Y.: Multi-Model Assessment of Stratospheric Ozone Return Dates and Ozone Recovery in CCMVal-2 Models, Atmos. Chem. Phys., 10, 9451-9472, https://doi.org/10.5194/acp-10-9451-2010, 2010.

Eyring, V., Harris, N., Rex, M., Shepherd, T. G., Fahey, D. W., Amanatidis, G. T., Austin, J., Chipperfield, M. P., Dameris, M., Forster, P., Gettelman, A., Graf, H. F., Nagashima, T., Newman, P. A., Pawson, S., Prather, M. J., Pyle, J. A., Salawitch, R. J., Santer, B. D., and Waugh, D. W.: A Strategy for Process-Oriented Validation of Coupled Chemistry-Climate Models, Bull. Amer. Meteorol. Soc., 86, 1117-1133, https://doi.org/10.1175/BAMS-86-8-1117, 2005.

Eyring, V., Lamarque, J. F., Hess, P., Arfeuille, F., Bowman, K., Chipperfield, M. P., Duncan, B.,

https://doi.org/10.5194/egusphere-2025-3636
Preprint. Discussion started: 8 August 2025

Fiore, A., Gettelman, A., Giorgetta, M. A., Granier, C., Hegglin, M., Kinnison, D., Kunze, M., Langematz, U., Luo, B., Martin, R., Matthes, K., Newman, P. A., Peter, T., Robock, A., Ryerson, T., Saiz-Lopez, A., Salawitch, R., Schultz, M., Shepherd, T. G., Shindell, D., Staehelin, J., Tegtmeier, S., Thomason, L., Tilmes, S., Vernier, J. P., Waugh, D. W., and Young, P. J.: Overview of IGAC/SPARC Chemistry-Climate Model Initiative (CCMI) Community Simulations in Support of Upcoming Ozone and Climate Assessments, SPARC Newsletter, 48-66, 2013.

Froidevaux, L., Anderson, J., Wang, H. J., Fuller, R. A., Schwartz, M. J., Santee, M. L., Livesey, N. J., Pumphrey, H. C., Bernath, P. F., Russell III, J. M., and McCormick, M. P.: Global OZone Chemistry and Related Trace Gas Data Records for the Stratosphere (GOZCARDS): Methodology and Sample Results with a Focus On HCl, H_2O, and O_3, Atmos. Chem. Phys., 15, 10471-10507, https://doi.org/10.5194/acp-15-10471-2015, 2015.

Froidevaux, L., Kinnison, D. E., Wang, R., Anderson, J., and Fuller, R. A.: Evaluation of CESM1 (WACCM) Free-Running and Specified Dynamics Atmospheric Composition Simulations Using Global Multispecies Satellite Data Records, Atmos. Chem. Phys., 19, 4783-4821, https://doi.org/10.5194/acp-19-4783-2019, 2019.

Gelaro, R., McCarty, W., Suárez, M. J., Todling, R., Molod, A., Takacs, L., Randles, C. A., Darmenov, A., Bosilovich, M. G., Reichle, R., Wargan, K., Coy, L., Cullather, R., Draper, C., Akella, S., Buchard, V., Conaty, A., Da Silva, A. M., Gu, W., Kim, G., Koster, R., Lucchesi, R., Merkova, D., Nielsen, J. E., Partyka, G., Pawson, S., Putman, W., Rienecker, M., Schubert, S. D., Sienkiewicz, M., and Zhao, B.: The Modern-Era Retrospective Analysis for Research and Applications, Version 2 (MERRA-2), J. Clim., 30, 5419-5454, https://doi.org/10.1175/JCLI-D-

https://doi.org/10.5194/egusphere-2025-3636
Preprint. Discussion started: 8 August 2025

16-0758.1, 2017.

Gettelman, A., Hegglin, M. I., Son, S. W., Kim, J., Fujiwara, M., Birner, T., Kremser, S., Rex, M., Anel, J. A., Akiyoshi, H., Austin, J., Bekki, S., Braesike, P., Bruhl, C., Butchart, N., Chipperfield, M., Dameris, M., Dhomse, S., Garny, H., Hardiman, S. C., Jockel, P., Kinnison, D. E., Lamarque, J. F., Mancini, E., Marchand, M., Michou, M., Morgenstern, O., Pawson, S., Pitari, G., Plummer, D., Pyle, J. A., Rozanov, E., Scinocca, J., Shepherd, T. G., Shibata, K., Smale, D., Teyssedre, H., and Tian, W.: Multimodel Assessment of the Upper Troposphere and Lower Stratosphere: Tropics and Global Trends, J. Geophys. Res.-Atmos., 115, https://doi.org/10.1029/2009JD013638, 2010.

Gettelman, A., Mills, M. J., Kinnison, D. E., Garcia, R. R., Smith, A. K., Marsh, D. R., Tilmes, S., Vitt, F., Bardeen, C. G., McInerny, J., Liu, H. L., Solomon, S. C., Polvani, L. M., Emmons, L. K., Lamarque, J. F., Richter, J. H., Glanville, A. S., Bacmeister, J. T., Phillips, A. S., Neale, R. B., Simpson, I. R., DuVivier, A. K., Hodzic, A., and Randel, W. J.: The Whole Atmosphere Community Climate Model Version 6 (WACCM6), J. Geophys. Res.-Atmos., 124, 12380-12403, https://doi.org/10.1029/2019JD030943, 2019.

Giorgetta, M. A.: Der Einfluß Der Quasi-Zweijährigen Oszillation Auf Die Allgemeine Zirkulation: Modellsimulationen Mit ECHAM4, phd, University of Hamburg, Hamburg, 1996.

Hanson, D. and Mauersberger, K.: Laboratory Studies of the Nitric Acid Trihydrate: Implications for the South Polar Stratosphere, Geophys. Res. Lett., 15, 855-858, https://doi.org/10.1029/GL015i008p00855, 1988.

Hauglustaine, D. A. and Ehhalt, D. H.: A Three-Dimensional Model of Molecular Hydrogen in the Troposphere, J. Geophys. Res.-Atmos., 107, https://doi.org/10.1029/2001JD001156, 2002.

https://doi.org/10.5194/egusphere-2025-3636
Preprint. Discussion started: 8 August 2025

Hauglustaine, D. A., Granier, C., Brasseur, G. P., and Megie, G.: The Importance of Atmospheric Chemistry in the Calculation of Radiative Forcing On the Climate System, J. Geophys. Res.-Atmos., 99, 1173-1186, https://doi.org/10.1029/93JD02987, 1994.

Hines, C. O.: Doppler-Spread Parameterization of Gravity-Wave Momentum Deposition in the Middle Atmosphere. Part 1: Basic Formulation, J. Atmos. Sol.-Terr. Phys., 59, 371-386, https://doi.org/10.1016/S1364-6826(96)00079-X, 1997a.

Hines, C. O.: Doppler-Spread Parameterization of Gravity-Wave Momentum Deposition in the Middle Atmosphere. Part 2: Broad and Quasi Monochromatic Spectra, and Implementation, J. Atmos. Sol.-Terr. Phys., 59, 387-400, https://doi.org/10.1016/S1364-6826(96)00080-6, 1997b.

Hoesly, R. M., Smith, S. J., Feng, L., Klimont, Z., Janssens-Maenhout, G., Pitkanen, T., Seibert, J. J., Linh, V., Andres, R. J., Bolt, R. M., Bond, T. C., Dawidowski, L., Kholod, N., Kurokawa, J., Li, M., Liu, L., Lu, Z., Moura, M. C. P., O'Rourke, P. R., and Zhang, Q.: Historical (1750-2014) Anthropogenic Emissions of Reactive Gases and Aerosols From the Community Emissions Data System (CEDS), Geosci. Model Dev., 11, 369-408, https://doi.org/10.5194/gmd-11-369-2018, 2018.

Holton, J. R., Haynes, P. H., McIntyre, M. E., Douglass, A. R., Rood, R. B., and Pfister, L.: Stratosphere-Troposphere Exchange, Rev. Geophys., 33, 403-439, https://doi.org/10.1029/95RG02097, 1995.

Horowitz, L. W., Naik, V., Paulot, F., Ginoux, P. A., Dunne, J. P., Mao, J., Schnell, J., Chen, X., He, J., John, J. G., Lin, M., Lin, P., Malyshev, S., Paynter, D., Shevliakova, E., and Zhao, M.: The GFDL Global Atmospheric Chemistry-Climate Model AM4.1: Model Description and Simulation Characteristics, J. Adv. Model. Earth Syst., 12,

https://doi.org/10.5194/egusphere-2025-3636
Preprint. Discussion started: 8 August 2025

https://doi.org/10.1029/2019MS002032, 2020.

Iacono, M. J., Delamere, J. S., Mlawer, E. J., Shephard, M. W., Clough, S. A., and Collins, W. D.: Radiative Forcing by Long-Lived Greenhouse Gases: Calculations with the AER Radiative Transfer Models, J. Geophys. Res.-Atmos., 113, https://doi.org/10.1029/2008JD009944, 2008.

Keeble, J., Hassler, B., Banerjee, A., Checa-Garcia, R., Chiodo, G., Davis, S., Eyring, V., Griffiths, P. T., Morgenstern, O., Nowack, P., Zeng, G., Zhang, J. K., Bodeker, G., Burrows, S., Cameron-Smith, P., Cugnet, D., Danek, C., Deushi, M., Horowitz, L. W., Kubin, A., Li, L. J., Lohmann, G., Michou, M., Mills, M. J., Nabat, P., Olivié, D., Park, S., Seland, O., Stoll, J., Wieners, K. H., and Wu, T. W.: Evaluating Stratospheric Ozone and Water Vapour Changes in CMIP6 Models From 1850 to 2100, Atmos. Chem. Phys., 21, 5015-5061, https://doi.org/10.5194/acp-21-5015-2021, 2021.

Kinne, S., O'Donnel, D., Stier, P., Kloster, S., Zhang, K., Schmidt, H., Rast, S., Giorgetta, M., Eck, T. F., and Stevens, B.: MAC-V1: A New Global Aerosol Climatology for Climate Studies, J. Adv. Model. Earth Syst., 5, 704-740, https://doi.org/10.1002/jame.20035, 2013.

Kirner, O., Ruhnke, R., Buchholz-Dietsch, J., Joeckel, P., Bruehl, C., and Steil, B.: Simulation of Polar Stratospheric Clouds in the Chemistry-Climate-Model EMAC Via the Submodel PSC, Geosci. Model Dev., 4, 169-182, https://doi.org/10.5194/gmd-4-169-2011, 2011.

Kovilakam, M., Thomason, L. W., Ernest, N., Rieger, L., Bourassa, A., and Millan, L.: The Global Space-Based Stratospheric Aerosol Climatology (Version 2.0): 1979-2018, Earth Syst. Sci. Data, 12, 2607-2634, https://doi.org/10.5194/essd-12-2607-2020, 2020.

Lamarque, J. F., Shindell, D. T., Josse, B., Young, P. J., Cionni, I., Eyring, V., Bergmann, D., Cameron-Smith, P., Collins, W. J., Doherty, R., Dalsoren, S., Faluvegi, G., Folberth, G., Ghan,

https://doi.org/10.5194/egusphere-2025-3636
Preprint. Discussion started: 8 August 2025

S. J., Horowitz, L. W., Lee, Y. H., MacKenzie, I. A., Nagashima, T., Naik, V., Plummer, D., Righi, M., Rumbold, S. T., Schulz, M., Skeie, R. B., Stevenson, D. S., Strode, S., Sudo, K., Szopa, S., Voulgarakis, A., and Zeng, G.: The Atmospheric Chemistry and Climate Model Intercomparison Project (ACCMIP): Overview and Description of Models, Simulations and Climate Diagnostics, Geosci. Model Dev., 6, 179-206, https://doi.org/10.5194/gmd-6-179-2013, 2013.

Lary, D. J. and Pyle, J. A.: Diffuse Radiation, Twilight, and Photochemistry — I, J. Atmos. Chem., 13, 373-392, https://doi.org/10.1007/BF00057753, 1991.

Lin, S. J. and Rood, R. B.: Multidimensional Flux-Form Semi-Lagrangian Transport Schemes, Mon. Weather Rev., 124, 2046-2070, https://doi.org/10.1175/1520-0493(1996)124<2046:MFFSLT>2.0.CO;2, 1996.

Lott, F.: Alleviation of Stationary Biases in a GCM through a Mountain Drag Parameterization Scheme and a Simple Representation of Mountain Lift Forces, Mon. Weather Rev., 127, 788-801, https://doi.org/10.1175/1520-0493(1999)127<0788:AOSBIA>2.0.CO;2, 1999.

Marti, J. and Mauersberger, K.: A Survey and New Measurements of Ice Vapor Pressure at Temperatures Between 170 and 250 K, Geophys. Res. Lett., 20, 363-366, https://doi.org/10.1029/93GL00105, 1993.

Matthes, K., Funke, B., Andersson, M. E., Barnard, L., Beer, J., Charbonneau, P., Clilverd, M. A., de Wit, T. D., Haberreiter, M., Hendry, A., Jackman, C. H., Kretzschmar, M., Kruschke, T., Kunze, M., Langematz, U., Marsh, D. R., Maycock, A. C., Misios, S., Rodger, C. J., Scaife, A. A., Seppala, A., Shangguan, M., Sinnhuber, M., Tourpali, K., Usoskin, I., De Kamp, M. V., Verronen, P. T., and Versick, S.: Solar Forcing for CMIP6 (V3.2), Geosci. Model Dev., 10, 2247-

https://doi.org/10.5194/egusphere-2025-3636
Preprint. Discussion started: 8 August 2025

2302, https://doi.org/10.5194/gmd-10-2247-2017, 2017.

Mauritsen, T., Bader, J., Becker, T., Behrens, J., Bittner, M., Brokopf, R., Brovkin, V., Claussen, M., Crueger, T., Esch, M., Fast, I., Fiedler, S., Flaeschner, D., Gayler, V., Giorgetta, M., Goll, D. S., Haak, H., Hagemann, S., Hedemann, C., Hohenegger, C., Ilyina, T., Jahns, T., Jimenez-de-la-Cuesta, D., Jungclaus, J., Kleinen, T., Kloster, S., Kracher, D., Kinne, S., Kleberg, D., Lasslop, G., Kornblueh, L., Marotzke, J., Matei, D., Meraner, K., Mikolajewicz, U., Modali, K., Moebis, B., Muellner, W. A., Nabel, J. E. M. S., Nam, C. C. W., Notz, D., Nyawira, S., Paulsen, H., Peters, K., Pincus, R., Pohlmann, H., Pongratz, J., Popp, M., Raddatz, T. J., Rast, S., Redler, R., Reick, C. H., Rohrschneider, T., Schemann, V., Schmidt, H., Schnur, R., Schulzweida, U., Six, K. D., Stein, L., Stemmler, I., Stevens, B., von Storch, J., Tian, F., Voigt, A., Vrese, P., Wieners, K., Wilkenskjeld, S., Winkler, A., and Roeckner, E.: Developments in the MPI-M Earth System Model Version 1.2 (MPI-ESM1.2) and its Response to Increasing CO2, J. Adv. Model. Earth Syst., 11, 998-1038, https://doi.org/10.1029/2018MS001400, 2019.

Meinshausen, M., Vogel, E., Nauels, A., Lorbacher, K., Meinshausen, N., Etheridge, D. M., Fraser, P. J., Montzka, S. A., Rayner, P. J., Trudinger, C. M., Krummel, P. B., Beyerle, U., Canadell, J. G., Daniel, J. S., Enting, I. G., Law, R. M., Lunder, C. R., O'Doherty, S., Prinn, R. G., Reimann, S., Rubino, M., Velders, G., Vollmer, M. K., Wang, R., and Weiss, R.: Historical Greenhouse Gas Concentrations for Climate Modelling (CMIP6), Geosci. Model Dev., 10, 2057-2116, https://doi.org/10.5194/gmd-10-2057-2017, 2017.

Miller, M. J., Palmer, T. N., and Swinbank, R.: Parametrization and Influence of Subgridscale Orography in General Circulation and Numerical Weather Prediction Models, Meteorol. Atmos. Phys., 40, 84-109, https://doi.org/10.1007/BF01027469, 1989.

https://doi.org/10.5194/egusphere-2025-3636
Preprint. Discussion started: 8 August 2025

Moebis, B. and Stevens, B.: Factors Controlling the Position of the Intertropical Convergence Zone On an Aquaplanet, J. Adv. Model. Earth Syst., 4, https://doi.org/10.1029/2012MS000199, 2012.

Morgenstern, O., Braesicke, P., O'Connor, F. M., Bushell, A. C., Johnson, C. E., Osprey, S. M., and Pyle, J. A.: Evaluation of the New UKCA Climate-Composition Model - Part 1: The Stratosphere, Geosci. Model Dev., 2, 43-57, https://doi.org/10.5194/gmd-2-43-2009, 2009.

Morgenstern, O., Giorgetta, M. A., Shibata, K., Eyring, V., Waugh, D. W., Shepherd, T. G., Akiyoshi, H., Austin, J., Baumgaertner, A., Bekki, S., Braesicke, P., Bruhl, C., Chipperfield, M. P., Cugnet, D., Dameris, M., Dhomse, S., Frith, S. M., Garny, H., Gettelman, A., Hardiman, S. C., Hegglin, M. I., Jockel, P., Kinnison, D. E., Lamarque, J. F., Mancini, E., Manzini, E., Marchand, M., Michou, M., Nakamura, T., Nielsen, J. E., Olivie, D., Pitari, G., Plummer, D. A., Rozanov, E., Scinocca, J. F., Smale, D., Teyssedre, H., Toohey, M., Tian, W., and Yamashita, Y.: Review of the Formulation of Present-Generation Stratospheric Chemistry-Climate Models and Associated External Forcings, J. Geophys. Res.-Atmos., 115, https://doi.org/10.1029/2009JD013728, 2010.

Morgenstern, O., Hegglin, M. I., Rozanov, E., O'Connor, F. M., Abraham, N. L., Akiyoshi, H., Archibald, A. T., Bekki, S., Butchart, N., Chipperfield, M. P., Deushi, M., Dhomse, S. S., Garcia, R. R., Hardiman, S. C., Horowitz, L. W., Joeckel, P., Josse, B., Kinnison, D., Lin, M., Mancini, E., Manyin, M. E., Marchand, M., Marecal, V., Michou, M., Oman, L. D., Pitari, G., Plummer, D. A., Revell, L. E., Saint-Martin, D., Schofield, R., Stenke, A., Stone, K., Sudo, K., Tanaka, T. Y., Tilmes, S., Yamashita, Y., Yoshida, K., and Zeng, G.: Review of the Global Models Used within Phase 1 of the Chemistry-Climate Model Initiative (CCMI), Geosci. Model Dev., 10, 639-671, https://doi.org/10.5194/gmd-10-639-2017, 2017.

https://doi.org/10.5194/egusphere-2025-3636
Preprint. Discussion started: 8 August 2025

Neu, J. L., Prather, M. J., and Penner, J. E.: Global Atmospheric Chemistry: Integrating Over Fractional Cloud Cover, J. Geophys. Res.-Atmos., 112, https://doi.org/10.1029/2006JD008007, 2007.

Nordeng, T. E.: Extended Versions of the Convective Parametrization Scheme at ECMWF and their Impact On the Mean and Transient Activity of the Model in the Tropics, ECMWF Technical Memoranda, 41, 1994.

Palmer, T. N., Shutts, G. J., and Swinbank, R.: Alleviation of a Systematic Westerly Bias in General Circulation and Numerical Weather Prediction Models through an Orographic Gravity Wave Drag Parametrization, Q. J. R. Meteorol. Soc., 112, 1001-1039, https://doi.org/https://doi.org/10.1002/qj.49711247406, 1986.

Pawson, S., Kodera, K., Hamilton, K., Shepherd, T. G., Beagley, S. R., Boville, B. A., Farrara, J. D., Fairlie, T., Kitoh, A., Lahoz, W. A., Langematz, U., Manzini, E., Rind, D. H., Scaife, A. A., Shibata, K., Simon, P., Swinbank, R., Takacs, L., Wilson, R. J., Al-Saadi, J. A., Amodei, M., Chiba, M., Coy, L., de Grandpré, J., Eckman, R. S., Fiorino, M., Grose, W. L., Koide, H., Koshyk, J. N., Li, D., Lerner, J., Mahlman, J. D., McFarlane, N. A., Mechoso, C. R., Molod, A., O'Neill, A., Pierce, R. B., Randel, W. J., Rood, R. B., and Wu, F.: The GCM-Reality Intercomparison Project for SPARC (GRIPS):: Scientific Issues and Initial Results, Bull. Amer. Meteorol. Soc., 81, 781-796, https://doi.org/10.1175/1520-0477(2000)081<0781:TGIPFS>2.3.CO;2, 2000.

Plummer, D., Nagashima, T., Tilmes, S., Archibald, A., Chiodo, G., Fadnavis, S., Garny, H., Josse, B., Kim, J., Lamarque, J., Morgenstern, O., Murray, L., Orbe, C., Tai, A., Chipperfield, M., Funke, B., Juckes, M., Kinnison, D., Kunze, M., Luo, B., Matthes, K., Newman, P. A., Pascoe, C., and Peter, T.: CCMI-2022: A New Set of Chemistry-Climate Model Initiative (CCMI)

https://doi.org/10.5194/egusphere-2025-3636
Preprint. Discussion started: 8 August 2025

Community Simulations to Update the Assessment of Models and Support Upcoming Ozone Assessment Activities, SPARC Newsletter, 2021.

Prather, M. J.: Photolysis Rates in Correlated Overlapping Cloud Fields: Cloud-J 7.3C, Geosci. Model Dev., 8, 2587-2595, https://doi.org/10.5194/gmd-8-2587-2015, 2015.

Rayner, N. A., Parker, D. E., Horton, E. B., Folland, C. K., Alexander, L. V., Rowell, D. P., Kent, E. C., and Kaplan, A.: Global Analyses of Sea Surface Temperature, Sea Ice, and Night Marine Air Temperature Since the Late Nineteenth Century, J. Geophys. Res.-Atmos., 108, https://doi.org/10.1029/2002JD002670, 2003.

Reick, C. H., Raddatz, T., Brovkin, V., and Gayler, V.: Representation of Natural and Anthropogenic Land Cover Change in MPI-ESM, J. Adv. Model. Earth Syst., 5, 459-482, https://doi.org/10.1002/jame.20022, 2013.

Rozanov, E. V., Schlesinger, M. E., and Zubov, V. A.: The University of Illinois, Urbana-Champaign Three-Dimensional Stratosphere-Troposphere General Circulation Model with Interactive Ozone Photochemistry: Fifteen-Year Control Run Climatology, J. Geophys. Res.-Atmos., 106, 27233-27254, https://doi.org/10.1029/2000JD000058, 2001.

Rozanov, E. V., Zubov, V. A., Schlesinger, M. E., Yang, F. L., and Andronova, N. G.: The UIUC Three-Dimensional Stratospheric Chemical Transport Model: Description and Evaluation of the Simulated Source Gases and Ozone, J. Geophys. Res.-Atmos., 104, 11755-11781, https://doi.org/10.1029/1999JD900138, 1999.

Sandu, A. and Sander, R.: Technical Note: Simulating Chemical Systems in Fortran90 and Matlab with the Kinetic PreProcessor KPP-2.1, Atmos. Chem. Phys., 6, 187-195, https://doi.org/10.5194/acp-6-187-2006, 2006.

https://doi.org/10.5194/egusphere-2025-3636
Preprint. Discussion started: 8 August 2025

Schröter, J., Rieger, D., Stassen, C., Vogel, H., Weimer, M., Werchner, S., Förstner, J., Pril, F., Reinert, D., Zängl, G., Giorgetta, M., Ruhnke, R., Vogel, B., and Braesicke, P.: ICON-ART 2.1: A Flexible Tracer Framework and its Application for Composition Studies in Numerical Weather Forecasting and Climate Simulations, Geosci. Model Dev., 11, 4043-4068, https://doi.org/10.5194/gmd-11-4043-2018, 2018.

Shindell, D. T., Rind, D., and Lonergan, P.: Increased Polar Stratospheric Ozone Losses and Delayed Eventual Recovery Owing to Increasing Greenhouse-Gas Concentrations, Nature, 392, 589-592, https://doi.org/10.1038/33385, 1998.

Stenke, A., Schraner, M., Rozanov, E., Egorova, T., Luo, B., and Peter, T.: The SOCOL Version 3.0 Chemistry-Climate Model: Description, Evaluation, and Implications From an Advanced Transport Algorithm, Geosci. Model Dev., 6, 1407-1427, https://doi.org/10.5194/gmd-6-1407-2013, 2013.

Stevens, B., Giorgetta, M., Esch, M., Mauritsen, T., Crueger, T., Rast, S., Salzmann, M., Schmidt, H., Bader, J., Block, K., Brokopf, R., Fast, I., Kinne, S., Kornblueh, L., Lohmann, U., Pincus, R., Reichler, T., and Roeckner, E.: Atmospheric Component of the MPI-M Earth System Model: ECHAM6, J. Adv. Model. Earth Syst., 5, 146-172, https://doi.org/10.1002/jame.20015, 2013.

Sukhodolov, T., Egorova, T., Stenke, A., Ball, W. T., Brodowsky, C., Chiodo, G., Feinberg, A., Friedel, M., Karagodin-Doyennel, A., Peter, T., Sedlacek, J., Vattioni, S., and Rozanov, E.: Atmosphere-Ocean-Aerosol-Chemistry-Climate Model SOCOLv4.0: Description and Evaluation, Geosci. Model Dev., 14, 5525-5560, https://doi.org/10.5194/gmd-14-5525-2021, 2021.

Sukhodolov, T., Rozanov, E., Ball, W. T., Bais, A., Tourpali, K., Shapiro, A. I., Telford, P.,

https://doi.org/10.5194/egusphere-2025-3636
Preprint. Discussion started: 8 August 2025

Smyshlyaev, S., Fomin, B., Sander, R., Bossay, S., Bekki, S., Marchand, M., Chipperfield, M. P., Dhomse, S., Haigh, J. D., Peter, T., and Schmutz, W.: Evaluation of Simulated Photolysis Rates and their Response to Solar Irradiance Variability, J. Geophys. Res.-Atmos., 121, 6066-6084, https://doi.org/10.1002/2015JD024277, 2016.

Telford, P. J., Abraham, N. L., Archibald, A. T., Braesicke, P., Dalvi, M., Morgenstern, O., O'Connor, F. M., Richards, N. A. D., and Pyle, J. A.: Implementation of the Fast-JX Photolysis Scheme (V6.4) Into the UKCA Component of the MetUM Chemistry-Climate Model (V7.3), Geosci. Model Dev., 6, 161-177, https://doi.org/10.5194/gmd-6-161-2013, 2013.

Tian, W. S. and Chipperfield, M. P.: A New Coupled Chemistry-Climate Model for the Stratosphere: The Importance of Coupling for Future O3-Climate Predictions, Q. J. R. Meteorol. Soc., 131, 281-303, https://doi.org/10.1256/qj.04.05, 2005.

Tiedtke, M.: A Comprehensive Mass Flux Scheme for Cumulus Parameterization in Large-Scale Models, Mon. Weather Rev., 117, 1779-1800, https://doi.org/10.1175/1520-0493(1989)117<1779:ACMFSF>2.0.CO;2, 1989.

van der A, R. J., Allaart, M. A. F., and Eskes, H. J.: Extended and Refined Multi Sensor Reanalysis of Total Ozone for the Period 1970–2012, Atmos. Meas. Tech., 8, 3021-3035, https://doi.org/10.5194/amt-8-3021-2015, 2015.

van Marle, M. J. E., Kloster, S., Magi, B. I., Marlon, J. R., Daniau, A., Field, R. D., Arneth, A., Forrest, M., Hantson, S., Kehrwald, N. M., Knorr, W., Lasslop, G., Li, F., Mangeon, S., Yue, C., Kaiser, J. W., and van der Werf, G. R.: Historic Global Biomass Burning Emissions for CMIP6 (BB4CMIP) Based On Merging Satellite Observations with Proxies and Fire Models (1750-2015), Geosci. Model Dev., 10, 3329-3357, https://doi.org/10.5194/gmd-10-3329-2017, 2017.

https://doi.org/10.5194/egusphere-2025-3636
Preprint. Discussion started: 8 August 2025

Wild, O., Zhu, X., and Prather, M. J.: Fast-J: Accurate Simulation of in- And Below-Cloud Photolysis in Tropospheric Chemical Models, J. Atmos. Chem., 37, 245-282, https://doi.org/10.1023/A:1006415919030, 2000.

Zhu, Z. P.: Middle Atmospheric Chemistry-Climate Model MACO Code and Simulation Data, Zenodo, https://doi.org/10.5281/zenodo.16452132, 2025.